

# **GOME2 on MetOp**

## **Follow-on analysis of GOME2 in orbit degradation**

### **Final Report**

**Prepared by:**

F. Azam and A. Richter

With contributions from:

M. Weber, S. Noël, and J. P. Burrows



University of Bremen FB1

P.O. Box 33 04 40

D-28334 Bremen

**Document:**           **Final Report**

Issue:                   Version 2.1 – Final

Issue Date: 28.09.2015

# Table of Contents

1	Executive Summary.....	4
1.2	Summary of activities .....	4
1.3	Main Conclusions .....	4
1.4	Main Recommendations.....	5
2	Study Setup.....	6
2.2	Introduction.....	6
2.3	Definition of analysis strategy .....	6
2.4	Selection of lv2 data products to be used.....	7
1.4	Selection of time periods to be analysed.....	7
1.5	Selection of regions to be analysed .....	7
1.6	Definition of diagnostics to be used .....	8
3	Degradation and time series analysis.....	9
2.1	GOME2 MetOp-B (GOME2-B) vs. GOME2 MetOp-A (GOME2-A) time series... 9	
3.2.1	NO <sub>2</sub> .....	10
3.2.2	BrO .....	11
3.2.3	O <sub>3</sub> .....	13
3.2.4	H <sub>2</sub> O .....	14
3.2.5	SO <sub>2</sub> .....	15
3.3	Intensity dependency.....	16
3.3.1	NO <sub>2</sub> .....	16
3.3.2	BrO .....	16
3.4	Scan angle dependent degradation.....	17
3.4.1	Scan angle dependent degradation GOME2-B.....	17
3.4.2	Scan angle dependent degradation GOME2-A.....	19
2.2	Evaluation of glyoxal drift.....	20
2.3	Evaluation of GOME2-B slit function .....	22
3.5	Summary and points to address.....	23
4	Investigation of NO <sub>2</sub> retrieval problems .....	24
4.2	Irradiance problem.....	24

4.3	Eta problem .....	27
4.4	Resolution problem.....	28
4.5	Summary .....	30
5	Evaluation of new AIRR for GOME2-A.....	31
6	Evaluation of different keydata sets for GOME2-B.....	34
6.2	New irradiometric response function .....	35
6.3	Unsmoothed keydata.....	35
6.4	Partial smoothing.....	36
6.5	No polarisation correction.....	37
6.5.1	Polarisation correction and NO <sub>2</sub> .....	37
6.5.2	Polarisation correction and BrO .....	38
6.5.3	Polarisation correction and OCIO.....	38
6.6	Threshold in polarisation correction.....	39
6.6.1	Polarisation threshold NO <sub>2</sub> .....	40
6.6.2	Polarisation threshold OCIO.....	40
7	Principal Component Analysis (PCA) of fitting residuals .....	41
7.2	Introduction.....	41
7.2.1	Degradation and Calibration - impact on lv2 products .....	41
7.2.2	Principal Component Analysis (PCA).....	42
7.3	Analysis strategy .....	42
7.4	Case studies.....	43
7.4.1	PCA of NO <sub>2</sub> fitting residuals .....	43
7.4.2	PCA of new dataset with improved key data.....	48
7.4.3	Impact of no polarization correction .....	50
7.4.4	Impact of low order polynomial on NO <sub>2</sub> .....	52
7.4.5	PCA of OCIO residuals .....	55
7.5	Summary .....	59
8	Appendix .....	61

# 1 Executive Summary

## 1.2 Summary of activities

In this study, several aspects of the GOME2 lv1 data quality were evaluated, mainly focusing on GOME2-B. The work comprises

- An analysis of the impact of degradation on GOME2-B lv2 products
- An evaluation of degradation, orbit, and calibration dependent features in GOME2-B lv2 data
- A detailed investigation of GOME2-B NO<sub>2</sub> fitting problems
- An evaluation of the new GOME2-A solar irradiance data
- A detailed analysis of the impact of several key-data changes on GOME2-B lv2 products
- A Principal components Analysis of the residuals of the key-data tests

**Disclaimer:** Please note that the level-2 retrieval results presented in this document are not reflecting the performance of the official level-2 products available from the O3MSAF at <http://o3msaf.fmi.fi> . Level-2 retrieval results presented here are tailored for studying the impact of the GOME-2 radiometric degradation. Operational GOME-2 level-2 products are often corrected for degradation effects, where applicable, and consequently show improved or different product stability and performance. For more details on the performance of the individual operational GOME-2 level-2 products please consult the validation reports and product quality monitoring pages available at <http://o3msaf.fmi.fi> .

## 1.3 Main Conclusions

- GOME2-A degradation has slowed down very much after the second throughput test
- GOME2-B degradation follows the GOME2-A path when considering the already reduced throughput at launch
- GOME2-B NO<sub>2</sub> retrievals at wavelengths > 460 nm suffer from artefacts which could be tracked down to Xe line contamination in GOME2-B irradiance data
- There is a scan angle dependent degradation creating similar residuals in both GOME2 instruments in channel 3
- GOME2-B slit function changes with orbit position, season, and age behave similar to those seen in GOME2-A, probably as result of temperature changes
- The new set of in-flight calibrated GOME2-A irradiance measurements removes most of the diffuser induced apparent seasonality in slant columns retrieved in channel 3 (NO<sub>2</sub>, glyoxal)
- Using lv1 data without polarisation correction leads to overall much poorer fits unless the eta keyfunction is included in the analysis. For many situations, including eta is sufficient to compensate polarisation effects but not for all.

However, there are also viewing conditions for which activation of polarisation correction actually reduces fit quality, in particular in channel 2 at low values of  $q$ .

- PCA analysis of fitting residuals obtained on data with different calibration settings provided insight in latitude, season, calibration and viewing angle dependent spectral structures. However, assignment to individual calibration steps or geophysical conditions proved difficult and overall the usefulness of these tests for improvements of lv1 calibration turned out to be rather limited.

#### 1.4 Main Recommendations

- The solar irradiance data used for GOME2-B DOAS fits in channel 3 should be calibrated using key-data obtained with the FEL lamp to avoid Xe contamination.
- The new AIRR for GOME2-A should be made available as it results in more consistent data at least for DOAS fits on  $\text{NO}_2$  and glyoxal. Validation with independent measurements is however needed to quantify the improvement.
- The change in instrumental function over the lifetime of the GOME2 instruments needs to be characterized continuously as it has the potential to impact on long-term trends. The magnitude of the effect depends on the specific application.
- Polarisation correction of GOME2-B is working well but not for all situations. Inclusion of the eta key-function in the fit improves the residuals in many cases. As problems appear to be linked to very low  $q$  values, possible problems in the formulation of the polarisation correction in these situations should be evaluated.
- A scan angle dependent degradation is observed in channel 3 which is similar in both GOME2 instruments and can be corrected by including an empirically determined pseudo cross-section in the fit. The fit can also be improved by including the eta keyfunction. It should be investigated in how far this could be compensated by a degradation correction on lv1 data.

## 2 Study Setup

### 2.2 Introduction

The GOME2 MetOp-B degradation study aims at the following objectives:

- To identify and quantify the impact of degradation on GOME2 MetOp-B lv2 data products
- To separate the different mechanisms of how degradation impacts on lv2 data (throughput loss, change in key data, change in calibration accuracy)
- To identify changes in key data as a result of degradation
- To make recommendations for the possible use of updated key data in GOME2 MetOp-B calibration
- To compare the observed degradation of GOME2 on MetOp-B lv2 data products with the degradation reported for GOME2 on MetOp-A
- To make recommendations on improvements in calibration and possibly on changes in lv2 processing

### 2.3 Definition of analysis strategy

The work closely followed the structure of the first GOME2 MetOp-A degradation study in the initial phases. The main difference is that large focus was placed on the key data impact evaluation as the study proceeded.

- The IUP Bremen scientific GOME2 lv2 data is used to investigate the impact of degradation
- The statistical analysis of trace gas columns from GOME2 MetOp-B over specific regions are used to study their degradation related changes over time. The results are compared with the simultaneous measurements from GOME2 MetOp-A to separate between real trends and degradation effects.
- Principal component analysis of fitting residuals is conducted on selected test cases to identify possible systematic spectral features introduced by degradation or arising from the calibration deficiencies and the approach adopted here has to be considered as experimental.
- Subsets of data calibrated with alternative and improved keydata provided by EUMETSAT are tested to inspect the impact of different calibration settings on the lv2 data products and their degradation over time. Where issues in calibration appear to be at the base of the problems, attempts are made to link the observations to specific steps in the calibration and if possible to improve the calibration.

- The results of the first GOME2 degradation study are used for comparisons.

## 2.4 Selection of lv2 data products to be used

Based on the experience from the first GOME2 degradation study, the full list of IUP lv2 data products is selected for use in the study. This includes products from channel 2 (SO<sub>2</sub>, O<sub>3</sub>, BrO, HCHO), channel 3 (two different NO<sub>2</sub> retrievals) and from channel 4 (H<sub>2</sub>O). The spectral ranges of the respective fitting windows are summarized in Table 1.

The impact of degradation on the different products varies strongly as the absorption strengths are very different (O<sub>3</sub> and H<sub>2</sub>O being strong absorbers, HCHO and BrO rather weak absorbers), the light intensity in channel 2 is smaller and the effects of degradation are more pronounced at shorter wavelengths. The case of SO<sub>2</sub> is special in the sense that SNR is low even shortly after launch and noise is dominated by shot noise and interference by ozone absorption.

Table 1: ranges of fitting windows

Data Product	Spectral Range (nm)	Channel
NO <sub>2</sub>	425.0 – 450.0	3
	425.0 – 497.0	
BrO	336.0 – 347.0	2
SO <sub>2</sub>	312.5 – 327.0	2
O <sub>3</sub>	326.6 – 334.5	2
H <sub>2</sub> O	688.0 – 700.0	4
HCHO	337.0– 353.0	2

## 1.4 Selection of time periods to be analysed

As in the first GOME2 degradation study, all data is used for the vertical/slant column analysis, starting in January 2007 for MetOp-A and in January 2013 for MetOp-B.

For the investigation of keydata and Principal Component Analysis, special days are selected in agreement with EUMETSAT requirements. The impact of new improved key data, provided by the EUMETSAT is investigated for the reference day of 24<sup>th</sup> April 2014.

## 1.5 Selection of regions to be analysed

While global data is available for all products, the GOME2 time series are investigated for a subset of geo-locations where natural or anthropogenic variations are minimum to assess the overall consistency and possible changes with time. Two sets of regions are selected in this regard. The first set comprises the Southern Pacific Ocean (25°S-15°S

and 150°W-110°W) and the Sahara Desert (20°N-30°N and 0°E-30°E). The second set is taken for a snow and ice scenario, a so called “Ice-and-Snow-Box” which is a combination of Greenland (70°N-75°N, 50°W-30°W) and the Antarctic (70°S-75°S, 130°E-150°E).

For the systematic analysis of residuals and investigations of the key data impact, measurements for selected days are studied, this is important as the keydata impacts may differ in certain viewing angles and among hemispheres.

## 1.6 Definition of diagnostics to be used

For the time series analysis, the choice of diagnostics to be used follows closely the first GOME2 degradation study. For the evaluation of the lv2 products, the following parameters were monitored:

The main quantity of interest is the vertical column (VC) which is deduced from the retrieved slant column (SC) through division by appropriate air mass factors (AMF). The VCs of the relevant species have been corrected with  $1/\cos(\text{los})$  for line of sight effects. The absolute value of the vertical column can be compared between results from different retrievals. The spread of the VCs is used as a measure of the effect of degradation on the precision of lv2 products, calculated as the standard deviation (root mean square, RMS). The assumption is that the scatter is dominated by measurement noise, not natural variability and that for certain background regions, it will not vary between years.

The effect of degradation on the fit quality of the retrieved species is examined by considering the scatter of the residuals for a wavelength region used for a given retrieval, expressed as Chisquare ( $\chi^2$  or ChiSq). The computation of the ChiSq for each trace gas is carried out the same way as done in the previous study on GOME2 MetOp-A which is summarized in Table 2. Here  $\chi^2$  and  $\mu_i$  are fitted and the measured optical depths respectively.  $\sigma_i$  is the standard deviation of the fitted parameters and  $n_p$  and  $n_d$  represent the degrees of freedom. The absolute value of the ChiSq depends on several aspects such as photon shot noise, instrument calibration, quality of the cross-sections used and effects not fully taken into account in the retrieval. The assumption underlying the analysis is that changes in ChiSq between instruments and years are dominated by the effects of throughput changes and degradation.

Table 2: Overview of chi-square as computed for GOME2 MetOp-B lv2 products.

Trace Gas	Residuals Estimate
NO <sub>2</sub> , BrO, SO <sub>2</sub>	$\chi^2 = \frac{1}{n-1} \sum_{i=1}^n (X_i - \mu_i)^2$
O <sub>3</sub>	$\chi^2 = \frac{1}{n} \sum_{i=1}^n (X_i - \mu_i)^2$
H <sub>2</sub> O	$\text{Error} = \frac{\sigma_{K,\chi}}{\sqrt{n_d - n_p}}$ $= \frac{\sqrt{\text{cov}(p_K, p_K)}}{n_d - n_p} \sqrt{\sum_{i=1}^n (X_i - \mu_i)^2}$

### 3 Degradation and time series analysis

Time series of key parameters (VC, RMS, ChiSq, INT) for all available IUP GOME2 MetOp-B lv2 products are created for selected regions to monitor changes linked to degradation. The same time series for MetOp-A is extended from the data set available from the first degradation study for direct comparison (same time period) and relative comparison (same time after launch) to evaluate similarities and differences between the two instruments so as to identify and investigate the problems and peculiarities in the time series in more detail to determine the origin.

A set of IUP level 2 products (NO<sub>2</sub>, BrO, O<sub>3</sub>, H<sub>2</sub>O and SO<sub>2</sub>) is checked for degradation signals i.e. signs of throughput loss using the methods outlined above. The time series of the earthshine fit window intensity are only available for NO<sub>2</sub>, BrO and SO<sub>2</sub>. The analysis is performed on monthly means in order to have sufficient statistics and clear figures.

#### 2.1 GOME2 MetOp-B (GOME2-B) vs. GOME2 MetOp-A (GOME2-A) time series

The time series of the different species for the two sets of regions under consideration are shown in Fig. 1 to Fig. 10 with the first set as Sahara desert (red) and the Pacific Ocean (dark blue) and the second one over Greenland (green) and Antarctica (light blue).

The upper panel of each figure shows the vertical column's (VC) time evolution. The second panel illustrates the scatter of the VCs as RMS. The third and fourth panels

depict the time series of the retrieval residuals ( $\chi^2$ ) and the retrieval intensity (INT) respectively.

### 3.2.1 NO<sub>2</sub>

Keeping in view the problem in NO<sub>2</sub> retrievals observed in previous GOME2 -B studies at IUP due to the fit as well as calibration issues, the NO<sub>2</sub> time series for the two sets of regions are examined for two retrievals (see Fig. 1 and Fig. 2), the standard (solid lines) and the corrected (dotted lines, only displayed here for the first year of GOME2-B). In the corrected fit, the mean residual of the NO<sub>2</sub> fit for a single orbit in Dec. 2012 is introduced as an additional cross-section which does not have an effect on the NO<sub>2</sub> columns but systematically improves the residuals. As is clear from the figures, compared to GOME2-A, the VC of GOME2-B is lower over the Pacific by the end of 2014, possibly as result of QBO and / or ENSO changes. The  $\chi^2$  values are higher with the standard retrieval compared to the corrected one (more evident in the Sahara-Pacific set), and in all cases, the quality of GOME2-B fit residuals is lower than those of the first GOME2 during its first two years (2007 and 2008). The RMS of the two instruments agrees and the fit window intensities of GOME2-B are a bit lower. GOME2-A shows some gradual loss of intensity for both sets from 2007 until Sep. 2009 which seems to stabilize afterwards pointing to a reduction in degradation which implies that the degradation effect slowed down after the 2<sup>nd</sup> throughput test (Sept. 2009).

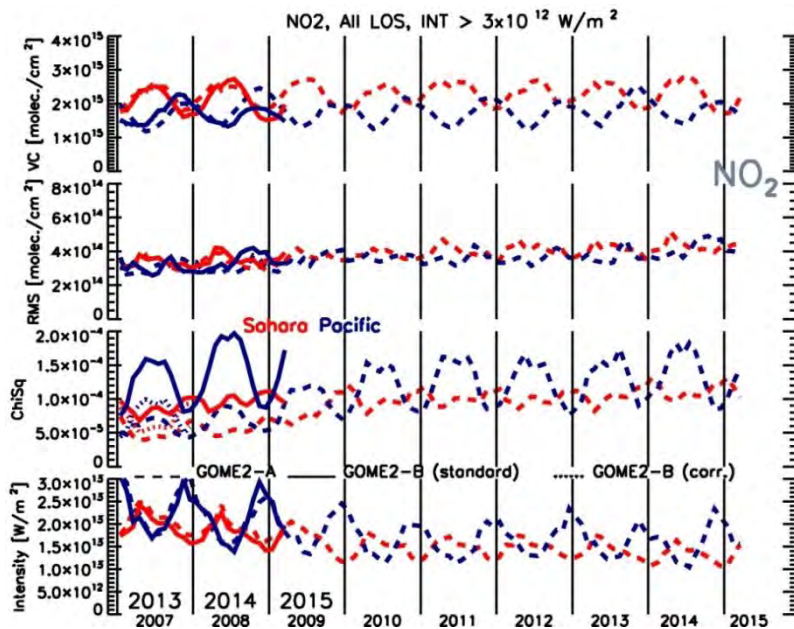


Fig. 1: GOME2 MetOp-B NO<sub>2</sub> time series of VC, RMS,  $\chi^2$ , and INT (top to bottom) for Jan. 2013- Dec. 2014 in comparison to the corresponding GOME2 MetOp-A time series (dashed lines) for Jan. 2007 – Dec. 2014. For GOME2 MetOp-B, the results are shown for two different NO<sub>2</sub> retrievals, the standard (solid lines) and the corrected (dotted lines, only shown here for 2013). The time series are plotted for the Sahara (red) and Pacific (blue) set

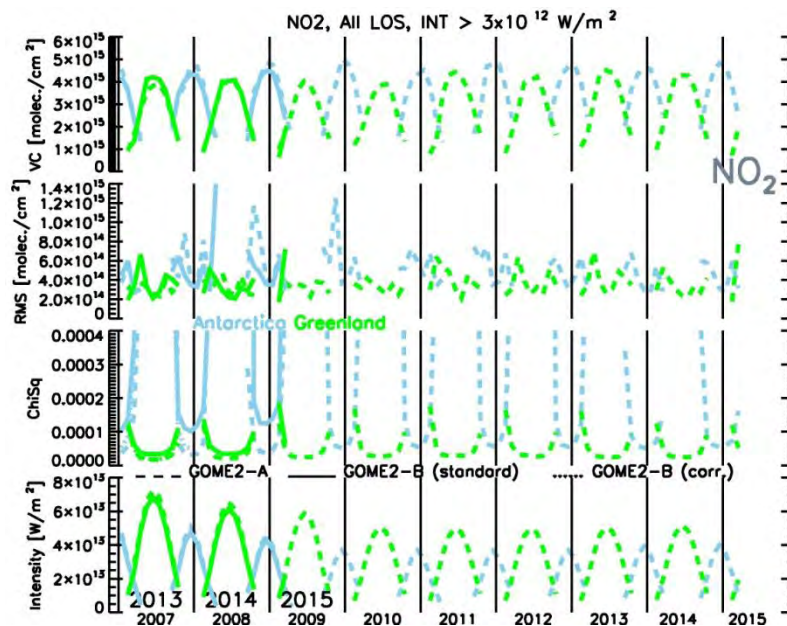


Fig. 2: Same as Fig. 1 but for the Antarctic (blue) and Greenland (green) set.

### 3.2.2 BrO

In the case of BrO, as is evident in Fig. 3, the GOME2-B time series of VC and intensity values generally follow the GOME2-A with the exception that the seasonality in VC of GOME2-B is opposite in Dec. for the Pacific. The RMS is a little higher for the former compared to the latter. For GOME2-A, the loss of accuracy and precision is more pronounced in the BrO time series compared to NO<sub>2</sub>. The retrieval of BrO, a weak absorber, relies on the strong earthshine signal to reduce the effect of shot noise and is therefore strongly affected by the loss of throughput that is degradation driven. The VCs and the RMS for both sets of geo-locations steadily increased until Sep. 2009 (Fig. 3 and Fig. 4) and stabilized afterwards, in line with the results for NO<sub>2</sub>. The  $\chi^2$  values also increase significantly with increasing seasonality until 2010. The fit window intensity is reduced by almost 50% between 2007 and 2010.

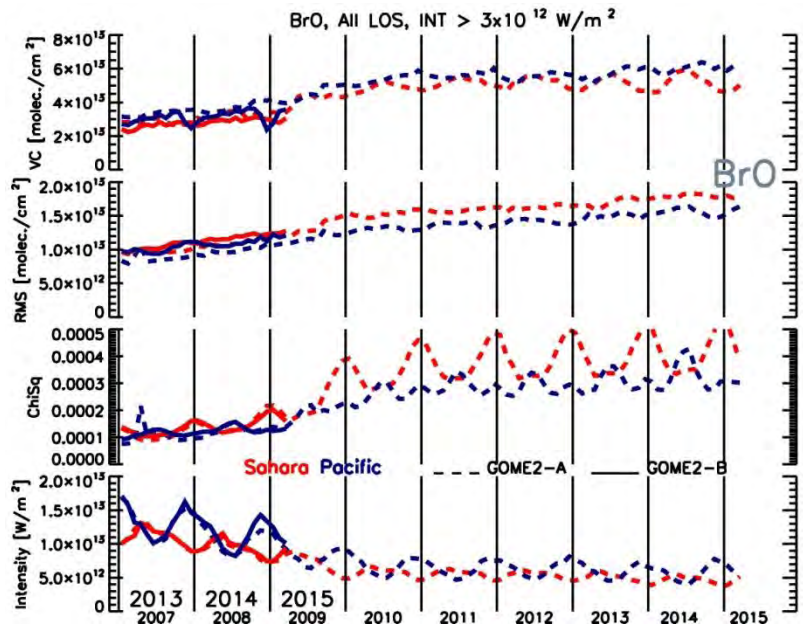


Fig. 3: Same as Fig. 1 but for BrO (using only standard retrieval for GOME2 MetOp-B).

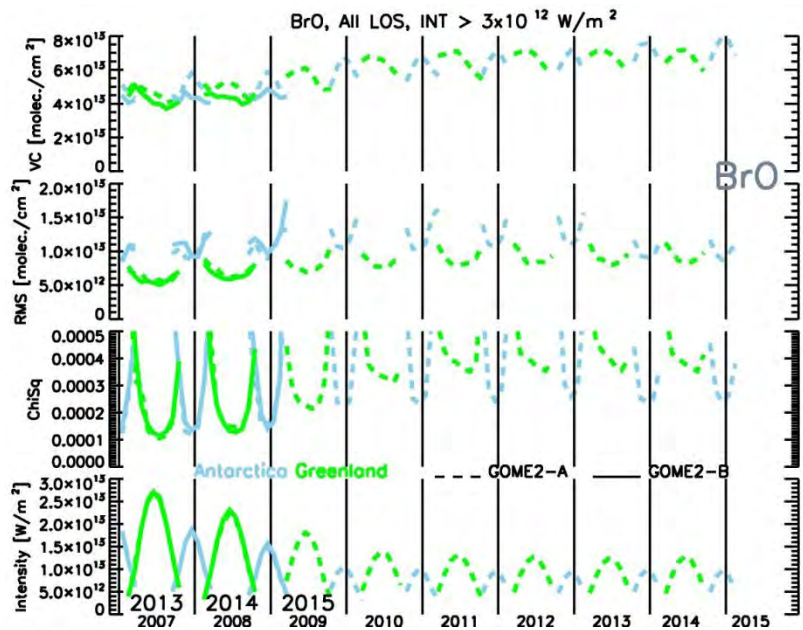


Fig. 4: Same as Fig. 2 but for BrO (using only standard retrieval for GOME2 MetOp-B).

### 3.2.3 O<sub>3</sub>

For O<sub>3</sub>, it can be seen in Fig. 5 and Fig. 6 that the quality of fit residuals for GOME2 MetOp-B is poorer than that for GOME2-A for both sets. Here, the stability of  $\chi^2$  after 2010 for GOME2-A is also evident.

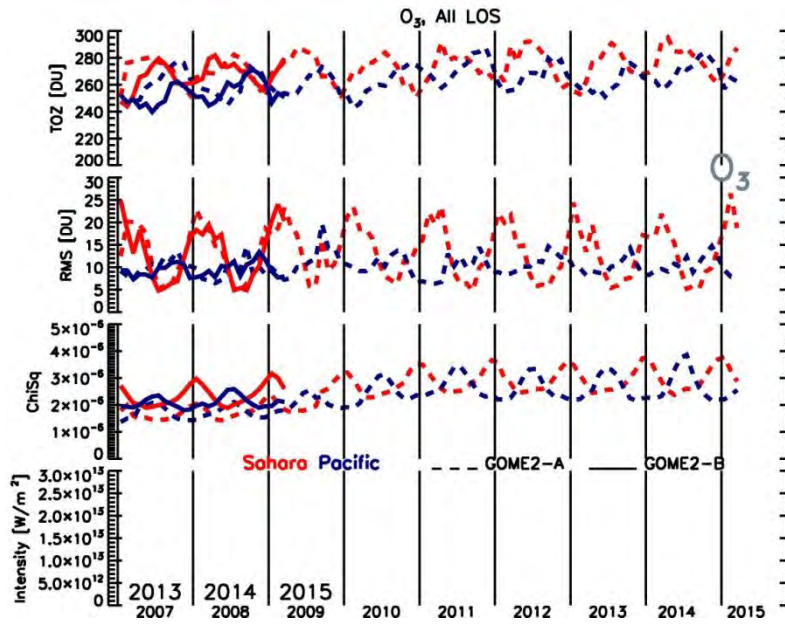


Fig. 5: Same as Fig. 3 but for O<sub>3</sub>. No information is available for intensity.

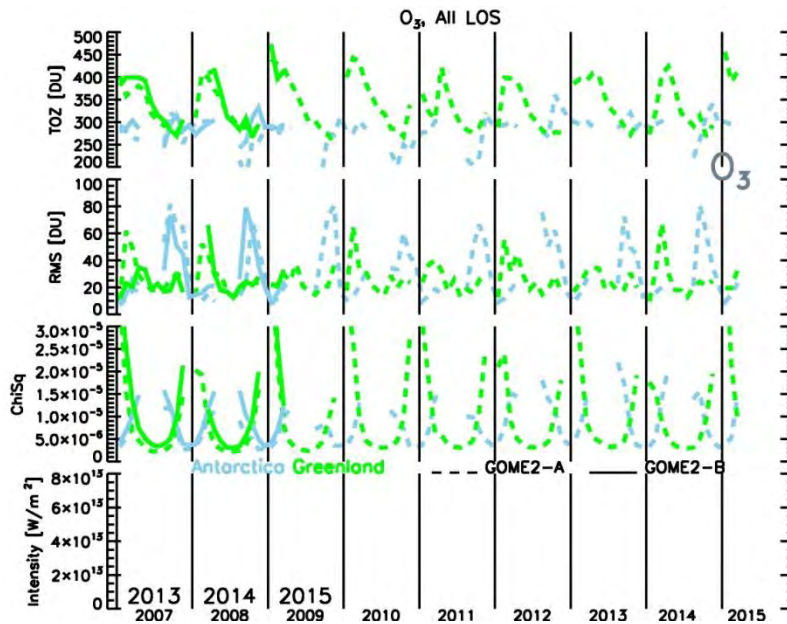


Fig. 6: Same as Fig. 4 but for O<sub>3</sub>. No information is available for the intensity.

### 3.2.4 H<sub>2</sub>O

The comparison of  $\chi^2$  of H<sub>2</sub>O for the two GOME2 instruments shows some interesting results for the two sets of geo-locations (see Fig. 7 and Fig. 8). The values for GOME2-B are higher than those for GOME2-A for the Sahara-Pacific set but lower for the Greenland-Antarctic set. This may point to problems with GOME2-B retrievals and needs to be further investigated.

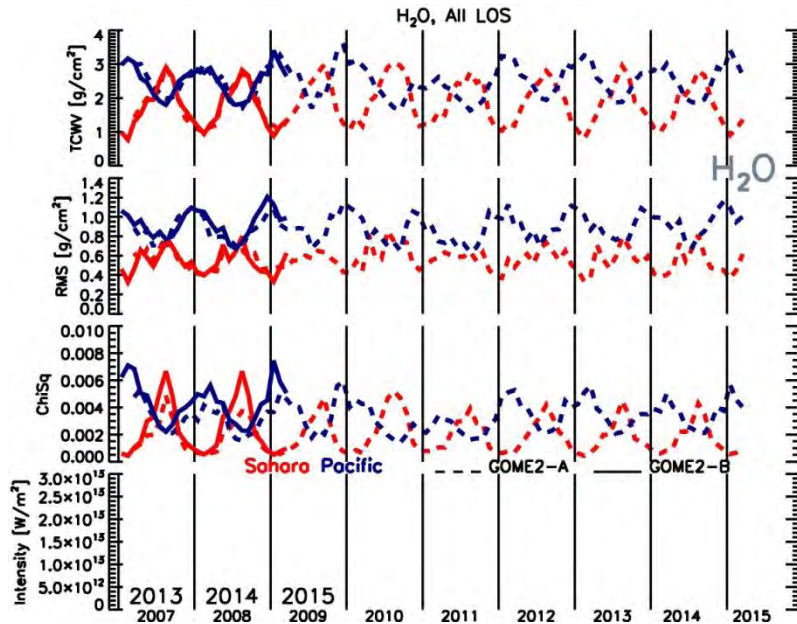


Fig. 7: Same as Fig. 3 but for H<sub>2</sub>O. No information is available for intensity.

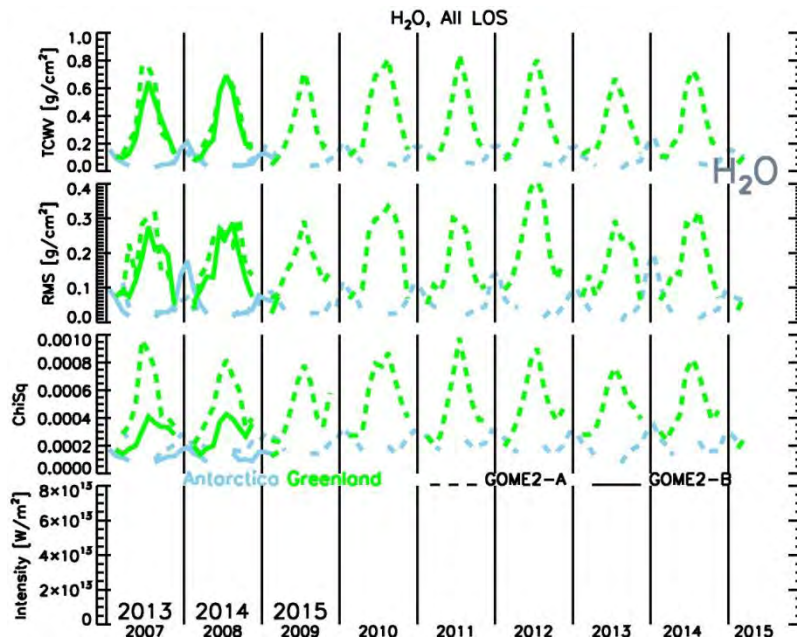


Fig. 8: Same as Fig. 4 but for H<sub>2</sub>O. No information is available for the intensity.

### 3.2.5 SO<sub>2</sub>

SO<sub>2</sub> slant columns i.e. SC and RMS for GOME2-B are smaller and flat compared to GOME2-A for the Pacific-Sahara region but are similar to the later for Greenland and Antarctica. SO<sub>2</sub> from volcanic eruptions during 2011 are visible in GOME2-A SC and RMS for the Sahara. GOME2-B shows more throughput loss for Antarctica. This inconsistency hints at a problem in the retrieval.

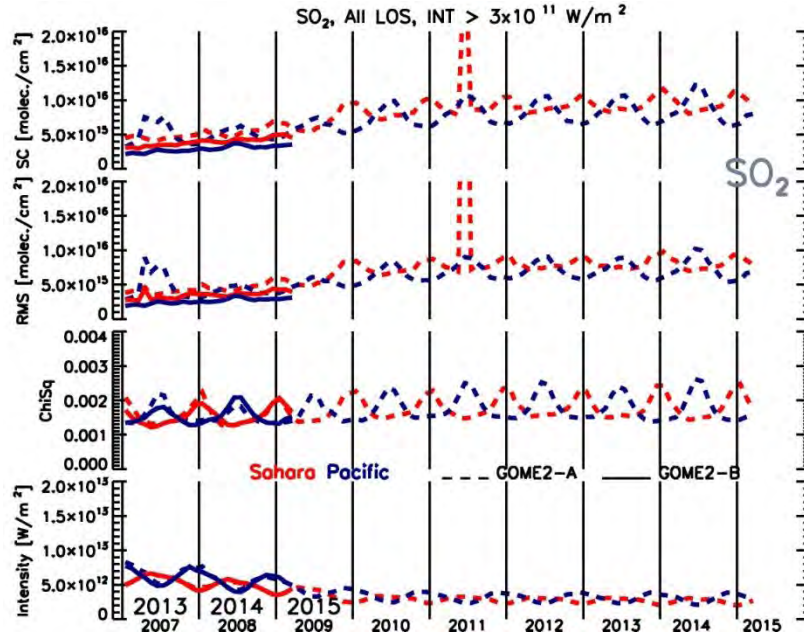


Fig. 9: Same as Fig. 3 but for SO<sub>2</sub>.

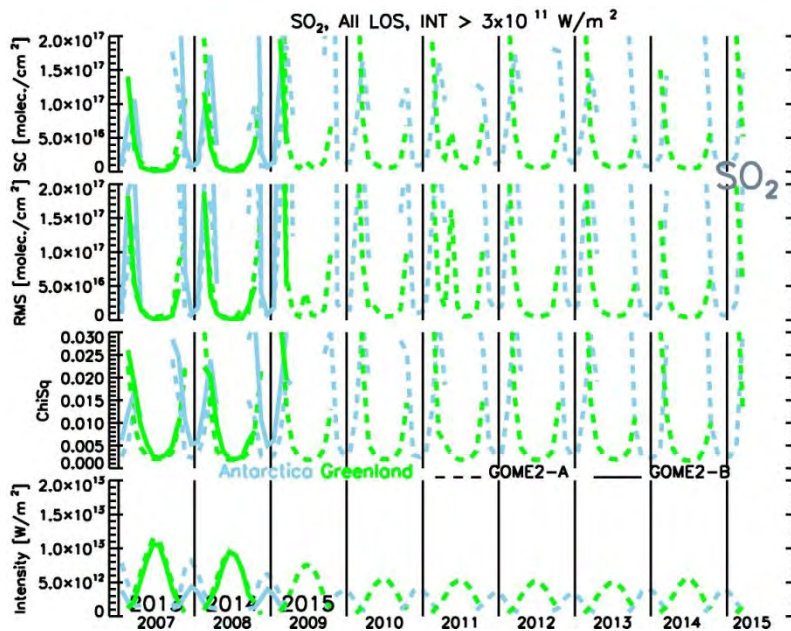


Fig. 10: Same as Fig. 4, but for SO<sub>2</sub>

### 3.3 Intensity dependency

The time series of DOAS products confirm that the fit window intensity loss for GOME2-B is following the GOME2-A path. For both GOME2 instruments, the dependency of ChiSq (residual scatter) on the fit window intensity is investigated for the NO<sub>2</sub> and BrO examples. The Sahara and Pacific regions are chosen and the results are displayed in Figs. 11 and 12 for NO<sub>2</sub> and BrO respectively, for every year since the launch, based on all data (and not the monthly means).

#### 3.3.1 NO<sub>2</sub>

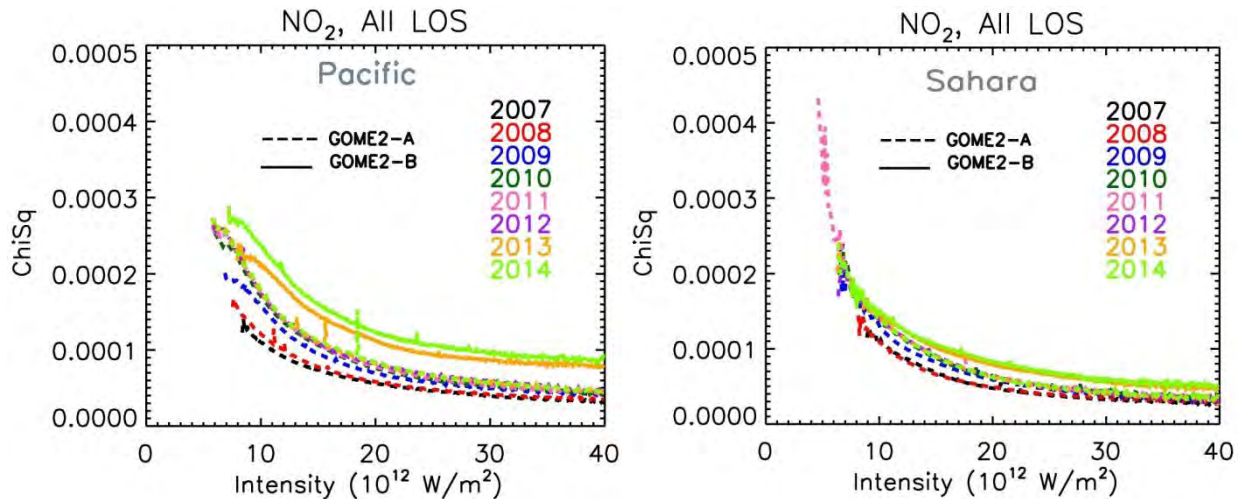


Fig. 11: Intensity dependency for ChiSq for GOME2-A (dashed lines) and GOME2-B (solid lines) NO<sub>2</sub> values over Pacific (left) and Sahara (right).

The standard retrieval for NO<sub>2</sub> is used for the analysis. The GOME2-B fit residuals are higher compared to GOME2-A and show an increase for the same intensity from 2013 to 2014 which is more pronounced in the Pacific region than the Sahara. This points at additional issues in GOME2-B retrievals that need improvement. For GOME2-A, the intensity vs. ChiSq pattern is quite similar for the years after the 2<sup>nd</sup> throughput test thereby supporting our previous conclusion of waning degradation related throughput loss.

#### 3.3.2 BrO

In the case of BrO, the ChiSq is higher for the same intensity as for NO<sub>2</sub>. The effect of the 2<sup>nd</sup> throughput test is also apparent here. The GOME2-B pattern fits the GOME2-A for its first two years of operation.

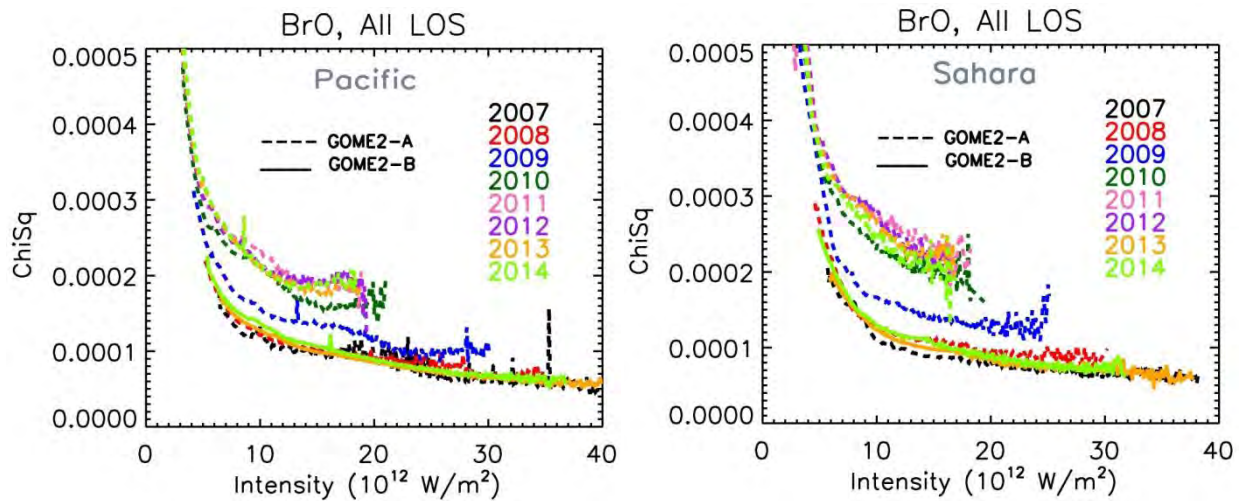


Fig. 12: Same as Fig. 11 but for BrO

### 3.4 Scan angle dependent degradation

At the beginning of GOME2-B data analysis, it became clear that in the large  $\text{NO}_2$  fitting window a smaller degree of polynomial could be used than for the same fit on GOME2-A data. Over time, this changed and a clear scan angle dependency developed. In the next two sections, this effect is analysed in more detail for both GOME2 instruments

#### 3.4.1 Scan angle dependent degradation GOME2-B

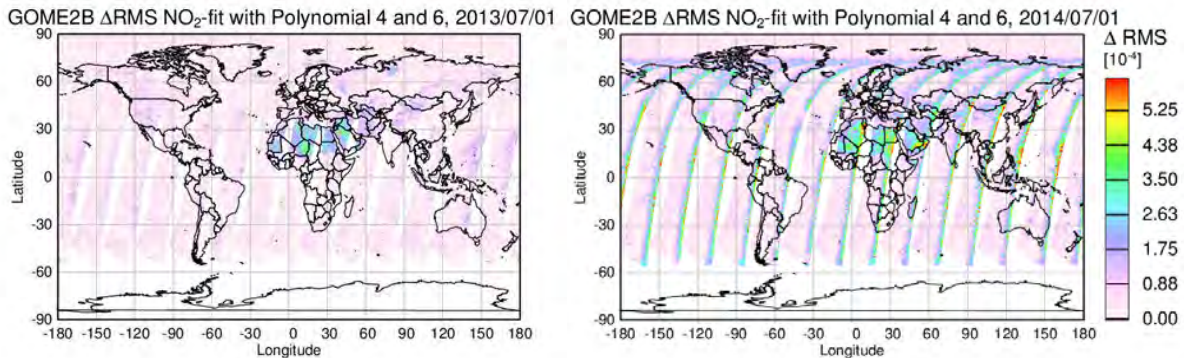


Fig. 13: Difference of GOME2-B  $\text{NO}_2$  fitting residuals in the large fitting window when using polynomial degrees of 6 and 4. Left: in July 2013, right: in July 2014

As shown in Fig. 13, GOME2-B fitting residuals in the 425 – 497 nm window did not depend on the degree of the polynomial in July 2013. The only exception is the Sahara region where the sand structure described in Richter et al., 2011 is better compensated when using a larger degree of the polynomial. One year later, there was a clear difference between the eastern and the western part of the scan, the eastern part having larger residuals at low degree of the polynomial. Taking the difference of the fitting residuals for the eastern and the western part of one orbit over the equatorial Pacific results in a smooth function as shown in Fig. 14. When this function is introduced into

the fit as an additional cross-section, the low order polynomial performs as well as the high order polynomial, again with the exception of desert regions (Fig. 15).

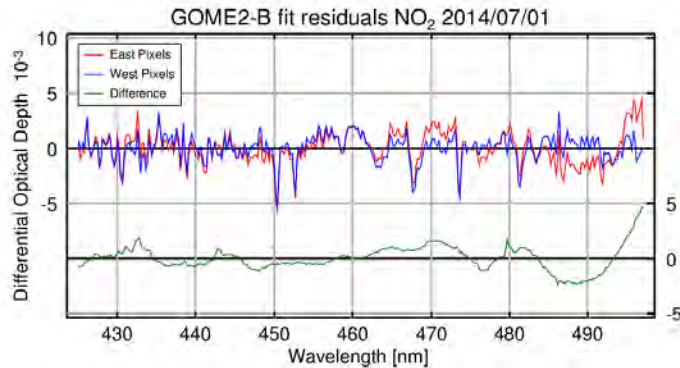


Fig. 14: Fitting residuals for east and west pixels (top) and difference (bottom).  
The difference can be used as empirical correction function

It is interesting to evaluate the temporal evolution of the fitting coefficient found for this empirical correction function by the DOAS retrieval. As can be seen in Fig. 15, there is a nearly linear increase in the coefficient found over the equatorial Pacific, indicating a gradual scan angle dependent degradation mainly affecting the eastern part of the scan. The apparent seasonality could be related to either non-linearities in the degradation or the well-known diffusor effect observed for many fitting parameters in GOME2 data.

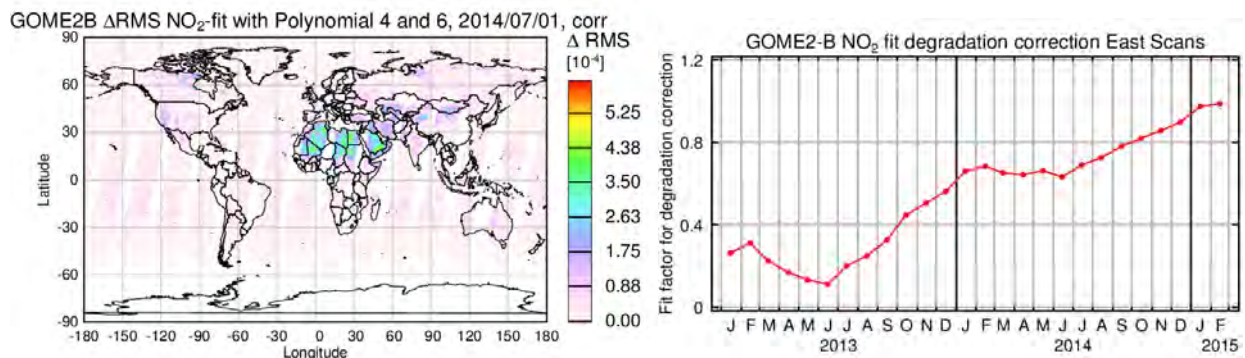


Fig. 15: Difference of residuals from fits using different polynomial degrees when including the scan angle correction function (left). Temporal evolution of the fit factor found for the correction function over the equatorial Pacific (right).

### 3.4.2 Scan angle dependent degradation GOME2-A

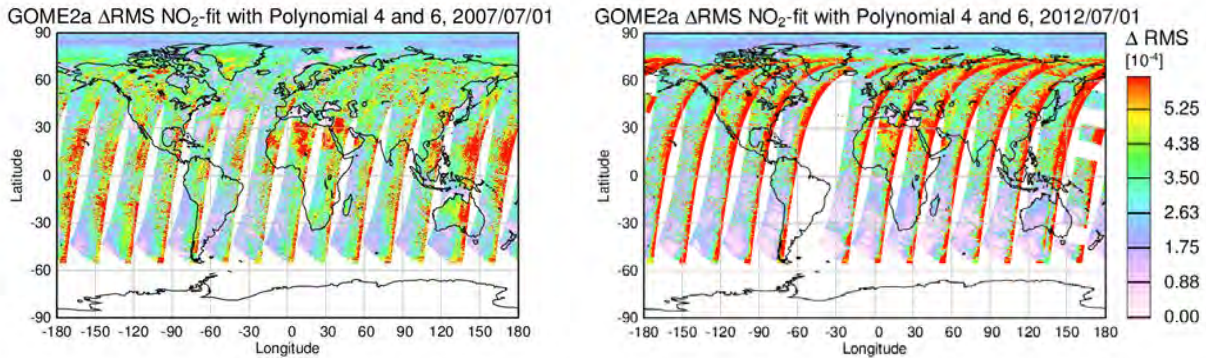


Fig. 16: As Fig. 13, but for GOME2-A and July 2007 (left) and July 2012 (right)

The same scan-angle analysis has also been performed on GOME2-A data. As shown in Fig. 16, the situation is different from that for GOME2-B in that the differences between the analyses using different polynomial degrees are larger, not limited to the eastern part of the scan and already apparent in the first year of operation. Nevertheless, the spectral structure of the difference in residuals is very similar for the two instruments (see Fig. 17), indicating the same origin of the effect. The more noisy results for GOME2-A are linked to the smaller difference between the eastern and western viewing directions. The source of the residuals is probably a polarisation dependent degradation or contamination of the scan mirror and is similar to the residuals observed when comparing forward modelled radiances with measurements. Some of these effects should be removed when applying the degradation model but this was not tested here.

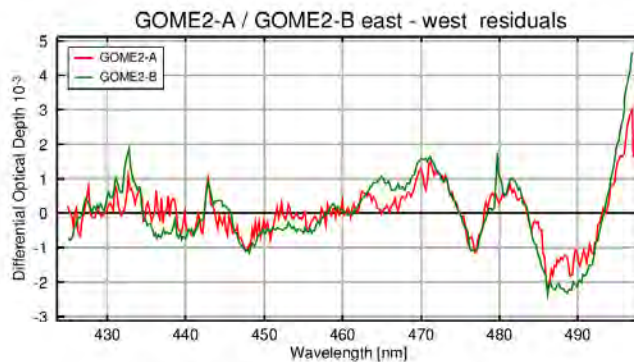


Fig. 17: Comparison of empirical scan angle dependency functions derived from GOME2-A and GOME2-B data

When including the GOME2-B retrieved correction function on GOME2-A data, the difference between the residuals from fits using different polynomial degrees vanishes as for GOME2-B (not shown). The GOME2-B function was selected as she appears less noisy and performs better in the fit.

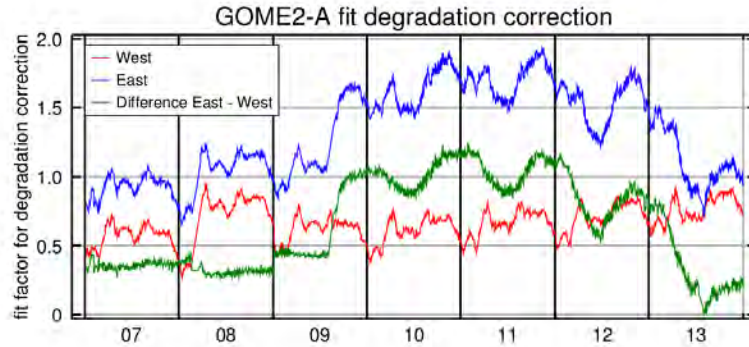


Fig. 18: Time evolution of fit factor found for scan angle correction function in GOME2-A data for east and west scans as well as their difference (in green).

The fitting coefficient of degradation function retrieved for GOME2-A over the equatorial Pacific behaves very different from that found for GOME2-B, indicating major differences in scan angle dependent degradation. For both east and west viewing directions, the fitting factor varies strongly with season and over time, probably because of the diffusor effect in combination with degradation. The difference between these two curves reveals nearly constant behaviour at the beginning of GOME2-A lifetime with steps linked to instrument changes. After the second throughput test, a smooth seasonal variation is observed, mainly driven by the eastern part of the scan and with large amplitude. Just before switching to the narrow swath, the difference between the viewing directions had reached a minimum. Values after this point cannot be directly compared as the viewing angles are smaller.

In summary, a scan angle dependent degradation is apparent in both GOME2 instruments in the 425 – 497 nm fitting window. The effect changes over time and in spite of having a very similar spectral signature in both instruments behaves differently over time. For the quality of DOAS products, it appears to be sufficient to use a higher degree of the polynomial to compensate the effect. No similar scan angle dependency could be identified in any of the other fitting windows.

## 2.2 Evaluation of glyoxal drift

Evaluation of GOME2-A glyoxal slant columns over the equatorial Pacific shows large drifts and seasonal variation (Fig. 19) while one would expect constant and very small columns. As the magnitude and variability of the glyoxal columns observed over the Pacific is larger than those over CHOCHO hotspots, usually a background correction is applied on the data subtracting the slant columns retrieved over the Pacific on the same day from all other measurements.

In order to identify the origin of the large glyoxal columns and their variability, a second DOAS analysis was performed where a constant solar background spectrum was used instead of the daily solar measurements. As seen in Fig. 19, the seasonality of the glyoxal columns disappears when using a fixed background spectrum, indicating that

this is explained by the diffuser problem on GOME2 solar observations. While from the point of view of seasonality the fixed background is to be preferred, it introduces degradation related drifts over time which are of a similar magnitude as the seasonality in the standard evaluation. Also, the fitting residuals are increasingly poorer as time increases between the observation and the day used as background.

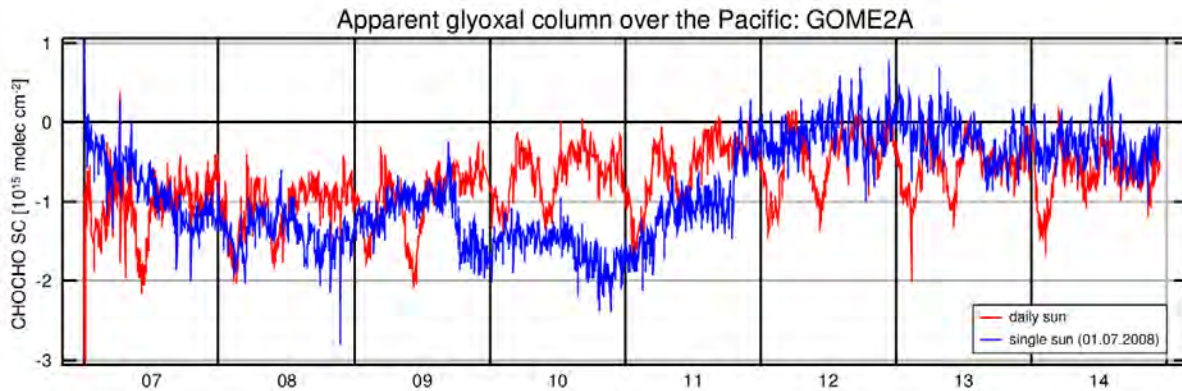


Fig. 19: Glyoxal columns retrieved over the equatorial Pacific using a) daily solar measurements as background (red) and b) a single solar background from July 1<sup>st</sup>, 2008

Interestingly, the data using the fixed background appear to have rapid changes during some times which are not visible in the analysis using daily background spectra. Comparison between results from GOME2-A, GOME2-B and OMI ( ) show that these variations are seen by all three instruments, and comparison with the MgII solar index confirms that these variations are linked to solar variations. This indicates a spectral interference between changes in the solar spectrum and glyoxal which cancel when using daily solar observations or earth-shine measurements from the same day as background.

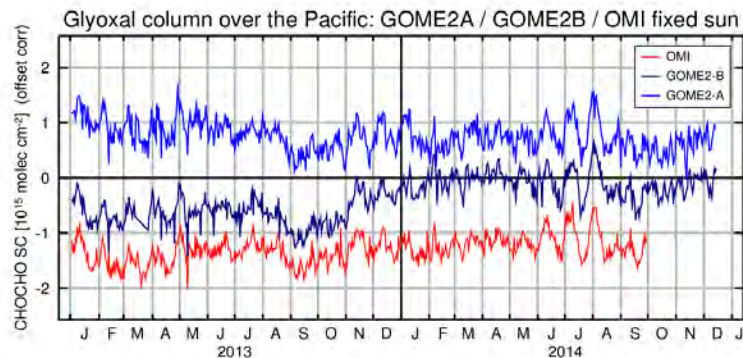


Fig. 20: Comparison of apparent glyoxal columns over the equatorial Pacific retrieved using fixed background spectra from data of GOME2-A, GOME2-B, and OMI.

## 2.3 Evaluation of GOME2-B slit function

As known from GOME2-A, the slit function of the GOME2 instruments changes with temperature of the optical bench and therefore has a small seasonality, a small variation over one orbit and at least in the case of GOME2-A also a long-term trend.

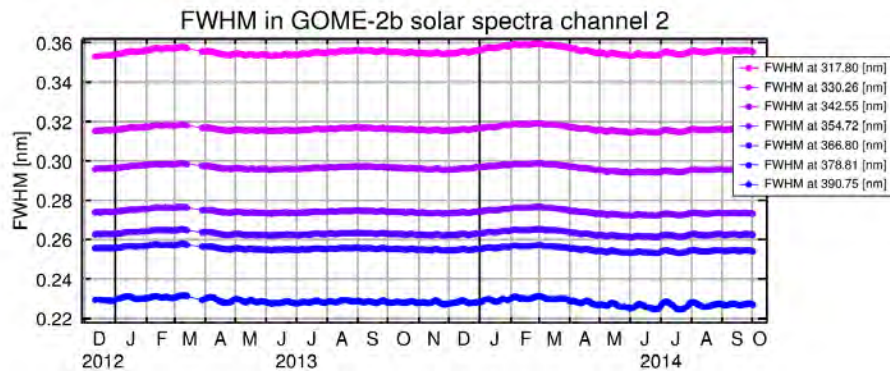


Fig. 21: Evolution of GOME2-B slit function FWHM in channel 2 as derived from irradiance measurements

The FWHM of the slit function can be determined by a non-linear fit of a Gaussian convolution with varying FWHM of a high resolution Fraunhofer atlas to the GOME2 measured irradiances. The result of such an analysis is shown in Fig. 21 for channel 2 and Fig. 22 for channel 3 of the GOME2-B instrument. In channel 2, the FWHM varies significantly over the channel with 0.355 nm at 318 nm and 0.23 nm at 390 nm. There also is a small seasonality and some interesting high frequency variations which are more pronounced at longer wavelengths. Overall the picture is quite similar to GOME2-A including the seasonality but the spread is somewhat larger and compared to GOME2-A, the downward trend appears to be smaller.

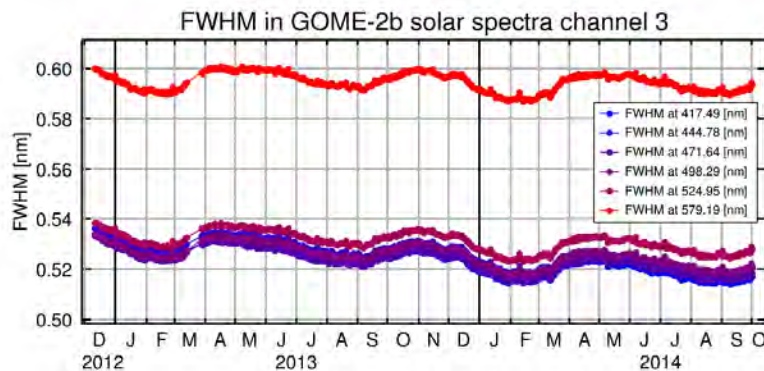


Fig. 22: Evolution of GOME2-B slit function FWHM in channel 3

In channel 3, the spread of values is smaller than in GOME2-A, in particular if the value at the right edge of the channel is excluded. The seasonality is more pronounced and different from than for GOME2-A. The downward trend is of similar magnitude in both instruments.

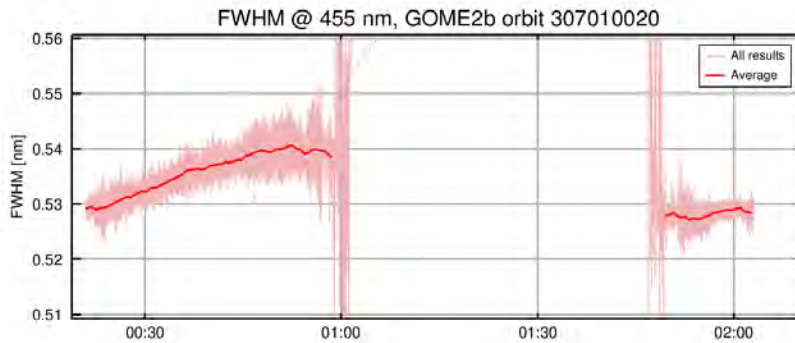


Fig. 23: Evolution of GOME2-B slit function FWHM at 455 nm along one orbit as derived from a DOAS fit

A similar convolution fit as for the irradiance data can also be applied to earth shine measurements. There is some interference between such a fit and variations in Ring effect, but if averaging is applied, a clear tendency can be retrieved. In Fig. 23, the results are shown for one individual orbit at 455 nm. It can be seen, that the FWHM increases along the orbit and changes back to the original value on the night side. The absolute value of the FWHM is very similar to that derived from the irradiance data; the variation over one orbit is of similar magnitude as the variation over one day. As the instrument warms on the illuminated side of the orbit, it appears that reducing temperatures result in reduced FWHM of the slit function in channel 3.

### 3.5 Summary and points to address

As a summary of this first comparison of degradation results between the two GOME2 instruments one can say that

- In general, the behaviour of GOME2-B so far is very similar to that of GOME2-A with respect to vertical columns retrieved, scatter of VCs, fitting residuals and intensity loss.
- The residuals of the NO<sub>2</sub> fit show a clear systematic problem which can be compensated to a large extent by including a mean residual from one randomly chosen orbit. The larger residual does not have an effect on the scatter of values. A detailed investigation of this effect is summarised in section 4.2.
- The BrO fits on GOME2-B data have similar residuals as for GOME2-A but show larger scatter, probably because of lower instrument throughput.
- The ozone fits are clearly poorer for GOME2-B but the scatter appears to be smaller. This indicates a probable systematic residual issue as in NO<sub>2</sub>, either linked to calibration issues or to incomplete removal of slit function dependencies.

- The H<sub>2</sub>O retrievals which for GOME2-A show very little signs of degradation. They behave unexpected in that the residuals are partly somewhat larger in GOME2 MetOp-B data but are significantly smaller over Greenland.
- The SO<sub>2</sub> SCs and RMS are flatter for GOME2-B. The intensities are smaller over the Antarctic region. It should be kept in mind that SO<sub>2</sub> is retrieved close to the channel boundary where loss of throughput is even higher having an adverse effect on the retrieval sensitivity.
- The small inconsistencies observed in O<sub>3</sub>, SO<sub>2</sub> and H<sub>2</sub>O hint at problems in the GOME2-B retrievals.
- GOME2-B is following the GOME2-A path of degradation as confirmed by the corresponding radiance signal of both instruments.
- For GOME2-A the overall degradation has slowed down or stabilized for all DOAS products after the second throughput test in Sep. 2009.
- There is a scan angle dependent degradation in both GOME2 instruments which has a very similar spectral signature but different temporal evolution. Correction in DOAS fits can be done by using a higher degree polynomial.
- There is a clear impact of changes in the irradiance spectra on glyoxal retrievals, but also an impact of real solar spectrum changes on the retrieved glyoxal columns.
- Spectral resolution of GOME2-B changes over each orbit and over one year, probably in response to temperature related mechanical changes of the instrument.

## 4 Investigation of NO<sub>2</sub> retrieval problems

At IUP Bremen, there are two different NO<sub>2</sub> fits performed on GOME2 data, one using the traditional 425 – 450 nm spectral window, and one applying an extended fitting range (425 – 497 nm). For GOME2 on MetOp-A, these two retrievals have very similar slant column results over background regions, the main differences being the reduced scatter in the large fitting window.

### 4.2 Irradiance problem

It soon became obvious, that when the same retrieval settings are applied to data from the second GOME2 instrument, a systematic constant offset appears between the two retrievals even in recent data (January 2014). This indicates that there is a retrieval problem in one or both of these spectral regions. Comparison with data from the first

GOME2 instrument and analysis of the line of sight dependence of the NO<sub>2</sub> results indicates that the offset is mainly in the results from the large fitting window.

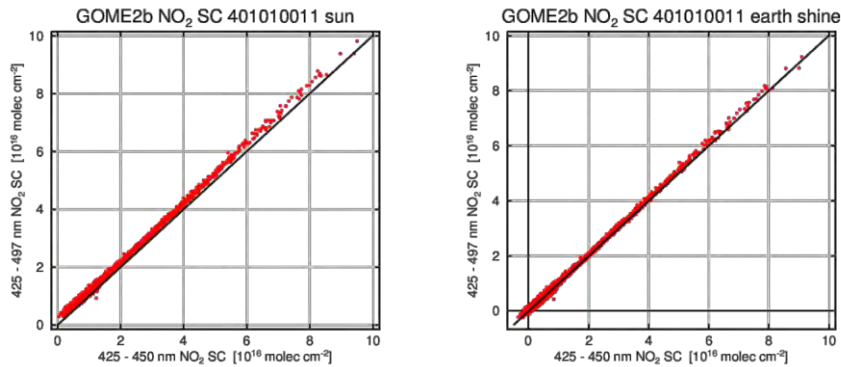


Fig. 24: Comparison of NO<sub>2</sub> slant columns for one orbit using the small fitting window (x-axis) and the large fitting window (y-axis). In the left panel, a solar irradiance is used as background, in the right panel an averaged earth-shine spectrum.

Surprisingly, the offset disappears when switching from a solar background spectrum to a background spectrum created by averaging over a large number of earth-shine spectra taken in the Pacific (see Fig. 24). From this it can be concluded, that either the problem is with the solar measurements or that exactly the same problem is present in all earth-shine data thus cancelling in the second test. While the latter possibility cannot be fully excluded, it is quite improbable.

When comparing the RMS of the two fitting windows, the large fitting window has much higher values when using the solar background. This again emphasises the fact that there appears to be a problem in the large fitting window. In line with the improvement in offset, most of the RMS difference disappears when using an earth shine background (Fig. 25). It is interesting to note that the fit residuals in the small fitting window are nearly identical for both backgrounds, indicating that the solar spectrum at least in the small fitting window is of good quality and that Ring correction in the retrievals is good (as Ring problems would affect the retrieval with solar background much more).

The conclusion from this analysis is, that something in the solar irradiance at wavelengths > 450 nm interferes with the NO<sub>2</sub> retrieval.

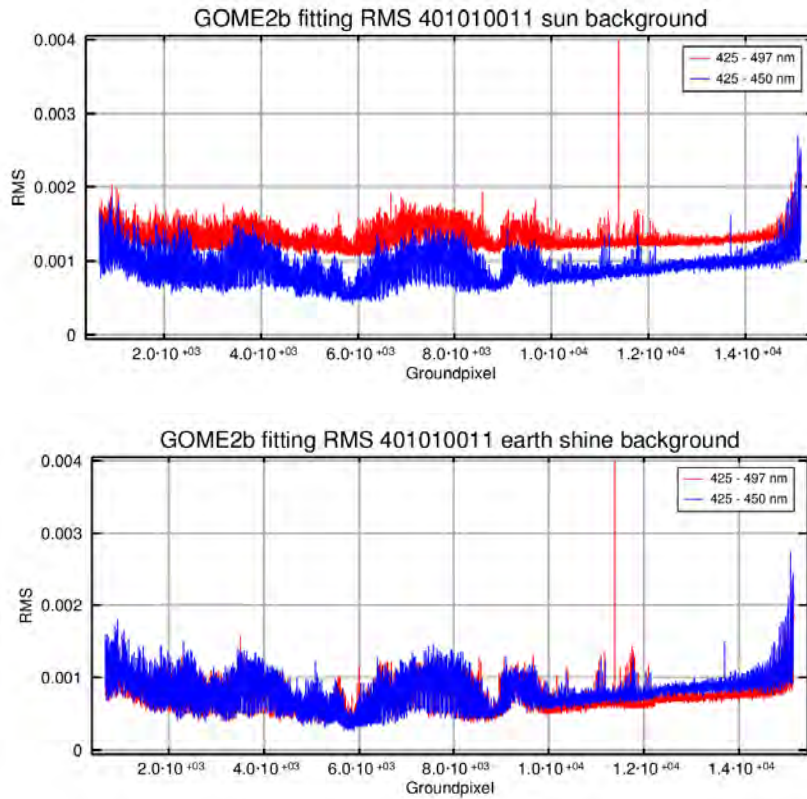


Fig. 25: RMS of NO<sub>2</sub> fit for one orbit of data using the two fitting windows (red and blue) and the two background spectra (upper and lower panel).

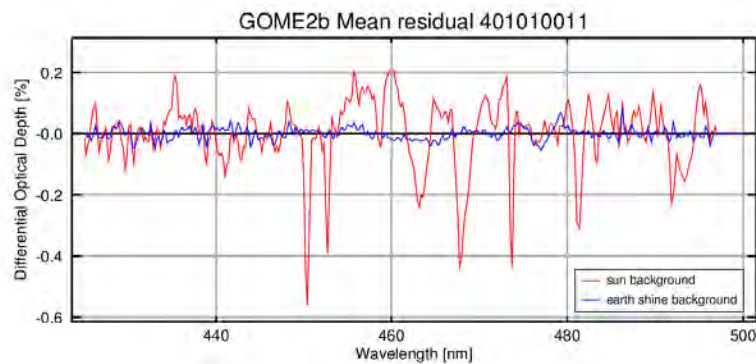


Fig. 26: Comparison of mean residuals for one orbit of NO<sub>2</sub> retrieval using either a solar irradiance (red) or an earth-she (blue) as background spectrum

In order to isolate this problem, the residual from the fit in the large fitting window has been averaged for the two cases, with solar irradiance and with earth-shine background. The results are shown in Fig. 26, and demonstrate the clear signature of a calibration problem, presumably linked to incomplete removal of Xenon lines in one or more of the calibration data sets used.

To clearly identify the source of the problem (radiance or irradiance spectra), additional tests have been performed. A first test is, to use GOME2-A instead of GOME2-B solar

data as background. In DOAS analysis, it is good practice always to use background spectra obtained using the same instrument as applied for the measurement itself. Use of other data leads to poor fits and systematic offsets in the retrieved columns. However, if a resolution correction is included in the fit (see section 4.4) and a high polynomial degree is used, acceptable fits are also possible on GOME2-B data when a GOME2-A solar measurement is used. As shown in Fig. 27, the noise in fitting residuals is larger if the GOME2-A irradiance is used but there is no indication for the systematic structures observed when using GOME2-B irradiances. This is clear evidence that (most of) the calibration problem lies with the irradiance, not with the radiance data.

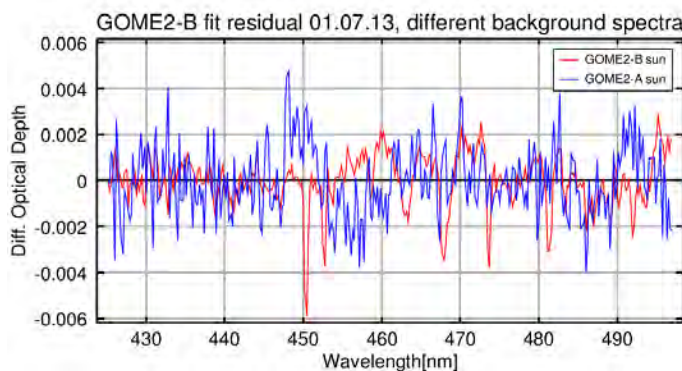


Fig. 27: Comparison of fitting residuals using GOME2-A (blue) and GOME2-B (red) irradiance measurements as background.

Finally, solar irradiance data using a different calibration based on the FEL irradiometric response key-data were provided by EUMETSAT for April 24, 2014 and as shown in Fig. 28, these data solve the problem with the persistent Xe residuals.

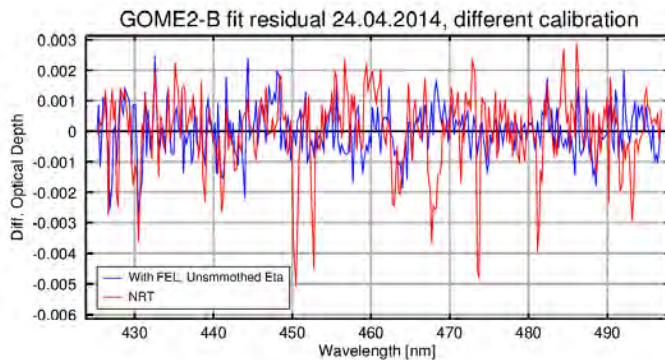


Fig. 28: Comparison of fitting residuals using the NRT irradiance (red) and the FEL calibrated irradiance (blue) as background. Note the different data as compared to previous figures.

### 4.3 Eta problem

Usually, a relatively high order polynomial is used in the NO<sub>2</sub> retrievals applying the large fitting window which is unfortunate as such a polynomial interferes with some

aspects of the retrieval. If a low order polynomial is used, large scan angle dependent residuals are observed as discussed in Section 3.4. This problem can be reduced by including the eta key function in the fit.

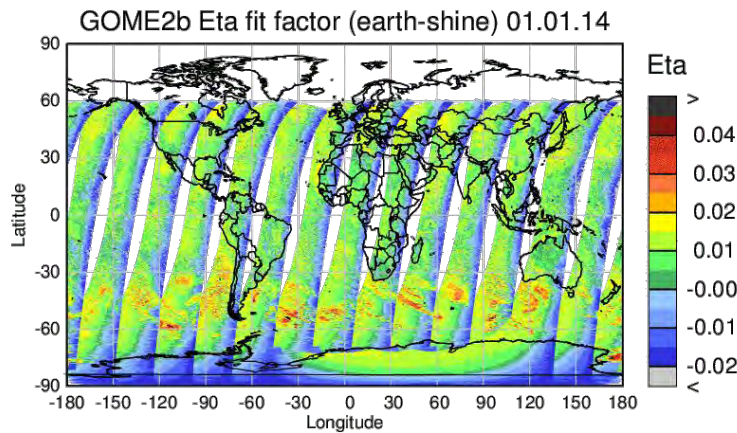


Fig. 29: Eta fit factor for a NO<sub>2</sub> fit in the large fitting window using a low order polynomial

The fitting coefficient retrieved for eta has a clear scan angle dependence (see Fig. 29) and in addition a seasonal variation. Interestingly, there is little signature of clouds in the distribution of the fit factor but some areas with high outliers which vary with season and might be linked to sun glint (to be confirmed). These results would hint at a general problem with polarisation calibration in this spectral region. An alternative explanation is that Eta compensates the increasing scan angle dependent degradation discussed in Section 3.4. In fact, the fit factor found for Eta increases over time, in line with the degradation findings. Therefore these results are not considered to provide strong evidence for problems in the polarisation correction.

#### 4.4 Resolution problem

Even when using an earth-shine background and eta in the fit, systematic structures remain in the residuals which have a high frequency structure. Comparison with an empirical spectral resolution correction derived from the Kurucz Fraunhofer atlas by taking the natural logarithm of the ratio of two spectra computed by using slightly different convolution of the high resolution spectrum (see Fig. 30) shows close agreement. Inclusion of the resolution correction as an additional cross-section in the retrieval improves the fit in both NO<sub>2</sub> windows, the effect being more pronounced in the larger fitting window. In fact, use of this correction brings the RMS from the two retrievals into excellent agreement (see Fig. 31).

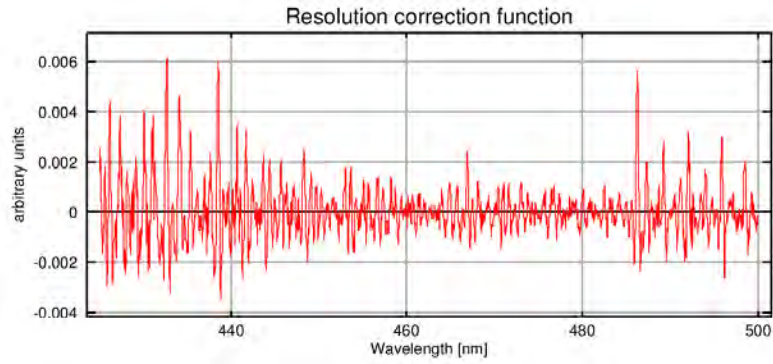


Fig. 30: Resolution correction derived from Kurucz Fraunhofer atlas

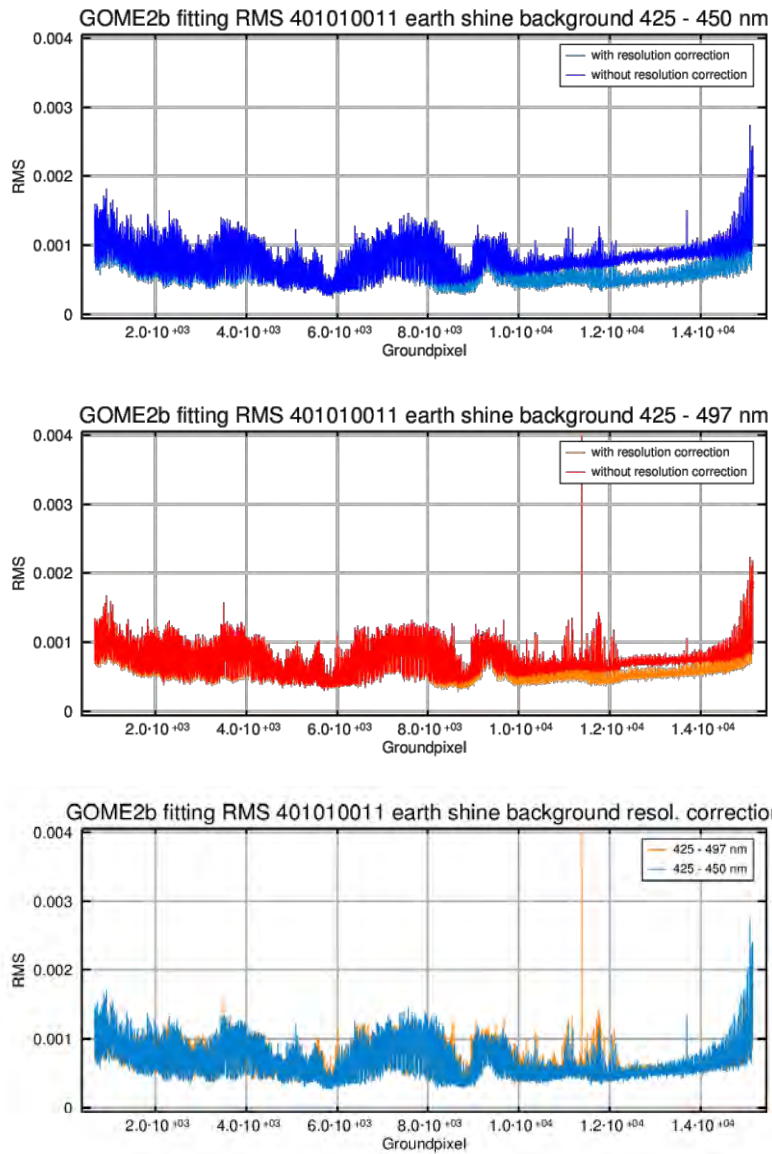


Fig. 31: Residual for NO<sub>2</sub> fits in the small (blue) and large (red) fitting windows with (light colours) and without (dark colours) resolution correction.

When plotting the improvement of fit residual obtained with the resolution correction, a clear hemispheric gradient is observed with large effects in the summer hemisphere at high latitudes and very small effects elsewhere (Fig. 32). There also appears to be some effect of clouds in the RMS difference but it is not very clear. It should be noted that the use of an earth-shine reference in Fig. 32 implies that there is a change of resolution along the orbit, not relative to the solar irradiance measurement.

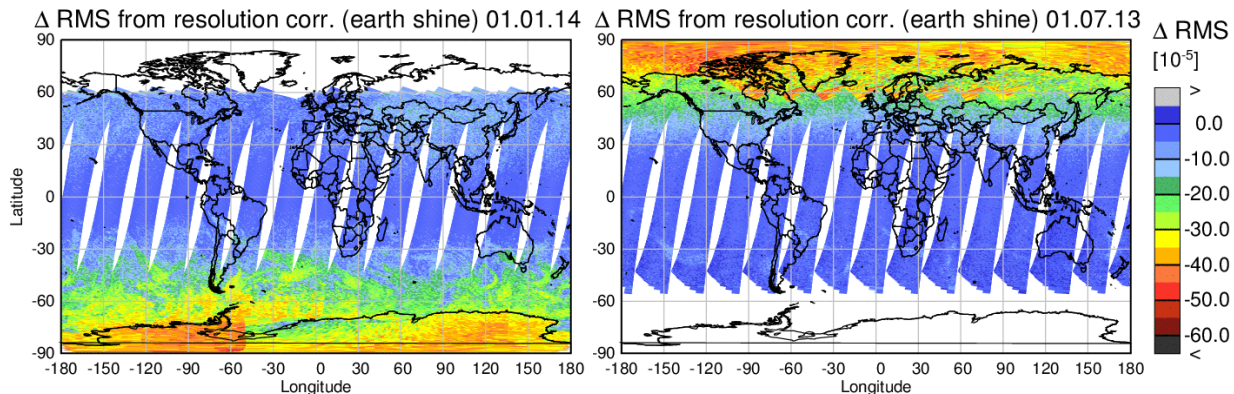


Fig. 32: Improvement in fit residual when including the resolution correction in a fit using earth-shine background spectrum for a day in January (left) and July (right)

This improvement by using a resolution correction indicates that the spectral resolution of the measurements changes over the orbit, and that the effect is largest in the summer hemisphere close to the poles. This is probably the effect of temperature changes over one orbit and closely linked to the resolution changes observed over the course of a year (see section 2.3).

#### 4.5 Summary

In summary, several problems have been identified in the NO<sub>2</sub> fit using the large window on GOME2-B data:

- The solar irradiance data of GOME2-B are contaminated by Xe-line residuals in the current NRT product. This leads to reduced fitting quality for NO<sub>2</sub> in the large fitting window and also to an offset in NO<sub>2</sub> columns.
- The spectral resolution of GOME2-B varies over one orbit and over the year, resulting in reduced quality of the retrievals if not corrected for with a correction cross-section. The impact on the NO<sub>2</sub> column is small 0.5% over one orbit, less than 1% over the first 2 years of GOME2-B operation) but could be relevant when trying to improve the fit for weak absorbers.
- Including the eta keydata function in the fit leads to systematic and scan angle dependent improvements, indicating incomplete polarisation calibration or degradation effects having spectral signatures which are similar to eta

## 5 Evaluation of new AIRR for GOME2-A

Already in early GOME data it was realised, that the choice of solar spectra used has a significant impact on the slant columns retrieved with DOAS type analysis, and that the impact varies systematically with season. This is not expected as the sun is relatively stable over time at least in the visible part of the spectrum (for deviations from this rule see also section 2.2). Further analysis showed, that the problem is related to the azimuthal dependence of the diffusor used for irradiance measurements. Switch to different diffuser types reduced the problem significantly in SCIAMACHY and GOME2, but some residual effects remain.

In this test, a revised set of irradiance measurements for GOME2-A is evaluated which has been calibrated for the azimuthal dependency using in-flight measurements. As result of problems with the wavelength calibration after the first years of GOME2-A operation, the wavelength calibration provided in the data was not used but instead the wavelength calibration of the very first measurement in the new irradiance data was applied to all days. It is expected, that this set of irradiance data does further reduce the diffuser impact on DOAS retrievals in GOME2-A data.

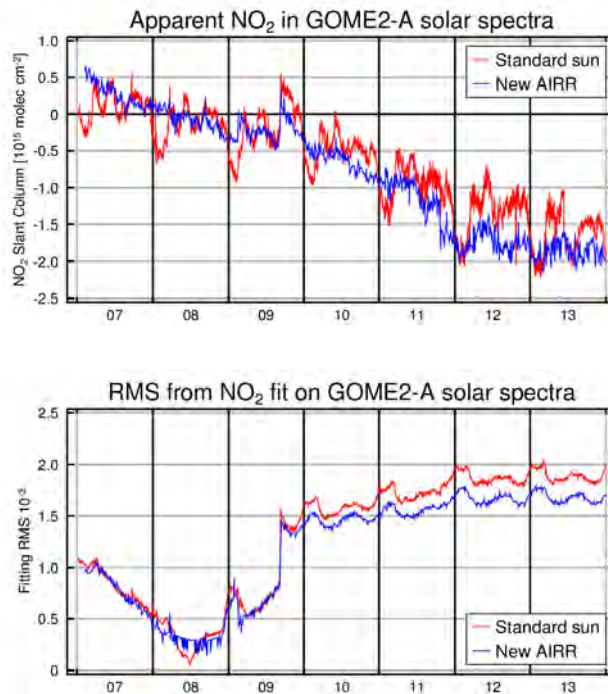


Fig. 33: Apparent  $\text{NO}_2$  (top) and fitting RMS (bottom) for retrievals on GOME2-A solar spectra using the NRT irradiance data (red) and the new AIRR data (blue)

In order to test the quality of the new irradiance data, a closed loop test was performed applying a DOAS retrieval on all irradiance spectra using one single solar spectrum from July 1<sup>st</sup>, 2008 as a background. This analysis should result in columns around 0 and any deviation from that indicates uncorrected effects of degradation or diffuser properties. As

shown in Fig. 33, the NRT solar spectra (“standard sun”) result in a clear seasonality of the retrieved (apparent) NO<sub>2</sub> columns. After the second throughput test, there is in addition an increased drift in these values. The new AIRR reduces the seasonality by more than a factor of two, indicating that the azimuthal dependence of the diffuser characteristics is better represented. With the azimuthal dependence removed, the degradation related trend becomes even more obvious. As can be seen in the time evolution of the fitting RMS (also Fig. 33), the new AIRR also results in slightly better fits at least for the years after 2009. The pronounced minimum in 2008 is linked to the choice of reference spectrum.

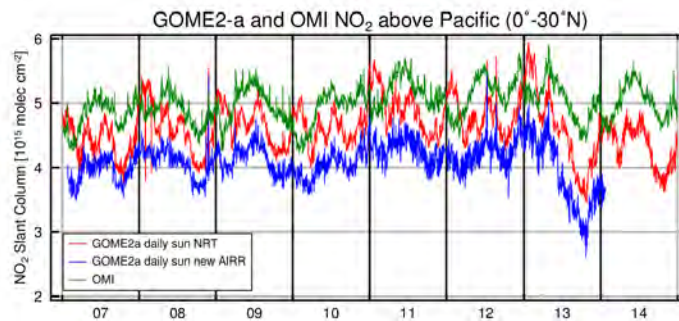


Fig. 34: NO<sub>2</sub> slant columns for GOME2-A earth shine spectra over the equatorial Pacific using the NRT irradiance data (red) and the new AIRR data (blue). OMI data are shown in green for comparison. Note that OMI overpass is later than GOME2-A overpass and therefore is expected to have slightly larger NO<sub>2</sub> slant columns.

In Fig. 34, a similar test is shown using earth-shine spectra over the equatorial Pacific instead of irradiance measurements. This test differs from the previous one as it is not a “closed loop” test where only irradiance spectra are used, but is applied to earth-shine data, representing real DOAS applications. As can be seen, NO<sub>2</sub> slant columns derived using the new AIRR data have a much reduced seasonality. They are also systematically lower than the original data and show more day-to-day variability, albeit at an amplitude much smaller than the seasonality present in the original data. Also shown in Fig. 34 are IUP OMI NO<sub>2</sub> slant columns which are slightly higher than the GOME2-A data but are in excellent agreement with the seasonality shown by the data retrieved with the new AIRR. In this context it has to be noted that the OMI analysis uses a single solar irradiance spectrum (see discussion in section 2.2).

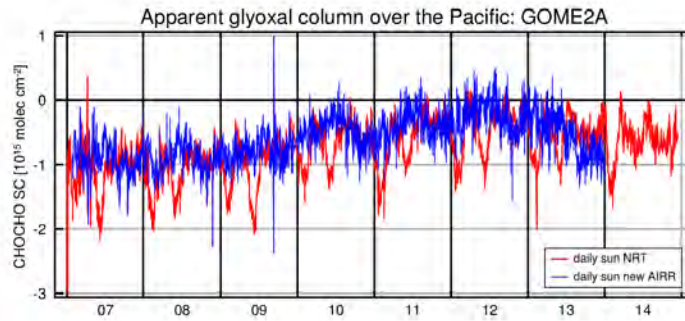


Fig. 35: Glyoxal slant columns for GOME2-A earth shine spectra over the equatorial Pacific using the NRT irradiance data (red) and the new AIRR data (blue).

It is interesting to check if a similar improvement as seen for  $\text{NO}_2$  is also found for a weak absorber such as glyoxal, for which a large apparent seasonality was discussed in section 2.2. In Fig. 35, glyoxal slant columns over the Pacific are shown for fits using both, the standard and the new AIRR. As for  $\text{NO}_2$ , most of the seasonality is removed but not the temporal drift. As glyoxal is a weak absorber, the increase in noise is even more visible than for  $\text{NO}_2$ .

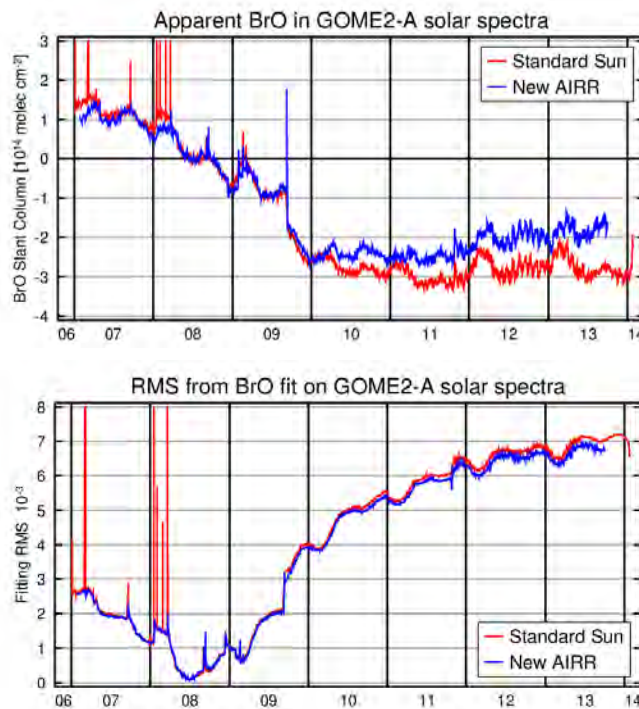


Fig. 36: As Fig. 33 but for BrO

Both  $\text{NO}_2$  and glyoxal are retrieved in GOME2 channel 3. In order to test the effect of the new AIRR in channel 2, the closed loop test was also performed on BrO data. As shown in Fig. 36, application of the new AIRR results in little change of the apparent BrO slant

Table 3: Overview on special keydata sets used in the study. ID is for IUP use only

Name	Description	ID
NewAIRR 05 <i>not used</i>	Smoothed on-ground key-data set 1.03 as applied after the 7 <sup>th</sup> of May 2013 but with the AIRR key-data exchanged by an in-orbit derived version with 0.5 degrees resolution in azimuth angle variation.	K1
NewAIRR 2 <i>not used</i>	Smoothed on-ground key-data set 1.03 as applied after the 7 <sup>th</sup> of May 2013 but with the AIRR key-data exchanged by an in-orbit derived version with 2.0 degrees resolution in azimuth angle variation.	K2
UnSmoothed	Key-data version 1.02 used as before the 7 <sup>th</sup> of May 2013, ie. the latest version of the on ground key-data for FM2 but without the FFT and spline- smoothing applied by EUMETSAT	K3
NoPol	Smoothed on-ground key-data set 1.03 as applied after the 7 <sup>th</sup> of May 2013 but the polarisation correction for main channel data has been turned off during the processing.	K4
NRT	NRT data for radiances but FEL calibrated irradiance	K5
No Eta Smooth <i>not used</i>	Original (smoothed) key-data but unsmoothed Eta	K6
Polarisation of at threshold	Smoothed keydata, polarisation correction switched off at $q < 0.05$	K7
With FEL No Eta Smooth	Eta unsmoothed, irradiance with FEL calibration	K8
AngularSmoothOnly	Key-data version 1.02 used as before the 7 <sup>th</sup> of May 2013, angular correction applied where appropriate, irradiance with FEL calibration	K9
AngularSmoothPlusXeFlt	Key-data version 1.02 used as before the 7 <sup>th</sup> of May 2013, angular correction applied where appropriate, filtering for Xe lines, irradiance with FEL calibration	K10

columns and a small improvement in fitting RMS. The apparent increase in BrO in the first months of each year is only slightly reduced with the new AIRR.

In summary, the new AIRR appears to remove most of the azimuthal dependency of the diffuser characteristics in channel 3, at least for NO<sub>2</sub> and glyoxal. Day-to-day variations are larger with the new AIRR, presumably because of uncertainties in the calibration procedure. As expected, the degradation related drift is not improved. In channel 2, no improvement was found.

## 6 Evaluation of different keydata sets for GOME2-B

In order to address some of the issues identified in GOME2-B retrievals, several sets of keydata were prepared by EUMETSAT and applied in the calibration of a full day of

measurements. By running DOAS fits on these modified datasets, it was hoped to gain insight into the role that individual calibration steps play in the DOAS fitting problems identified.

Several different settings were evaluated based on intermediate results obtained during the study. A short description is listed in Table 3. For all data sets, April 24, 2014 has been selected as test day. The quality of different lv1 data sets was then evaluated by performing standard DOAS fits, mostly of NO<sub>2</sub> but also of other species where indicated and comparing the fitting RMS to a reference retrieval, usually a fit on NRT data.

## 6.2 New irradiometric response function

One of the main conclusions from this study and earlier tests is that the current NRT irradiance spectra of GOME2-B are contaminated by Xe lines from the lamp used during calibration (see section 4.2). While for the radiance spectra, clear improvements have been achieved using smoothed and filtered keydata as already implemented in current NRT data, irradiance spectra continue to be affected.

As shown in section 4.2, the solar irradiance spectra distributed with the NRT data are contaminated by residual Xe emission lines in the keydata. A special solar irradiance spectrum has been provided by EUMETSAT for April 24, 2014 which was calibrated using the FEL based radiometric calibration data and does not present the Xe issue. From the point of view of NO<sub>2</sub> retrievals in the large fitting window, these irradiance spectra are to be preferred over the current NRT ones and therefore will be used in all subsequent tests. It should be noted that for other products such as aerosol absorbing index, this choice might not be the best.

Most of the tests on alternate keydata including spectra with alternative irradiometric calibration executed during the project were not performed on the FEL calibrated irradiances. These tests will not be discussed in the following as they are influenced by the irradiance problem. Instead, all tests have been performed using the solar irradiance provided in data set K8 (see Table 3 for scenario definitions), including the data set labelled NRT.

## 6.3 Unsmoothed keydata

On May 7, 2013, a new set of keydata was introduced in GOME2-B lv1 processing where spectral smoothing using an FFT algorithm has been applied to reduce the impact of residual Xe lines in the keydata. In order to evaluate the effectiveness of this smoothing approach, NO<sub>2</sub> retrievals were performed on a lv1 data set calibrated without smoothing, and differences in fitting RMS are compared.

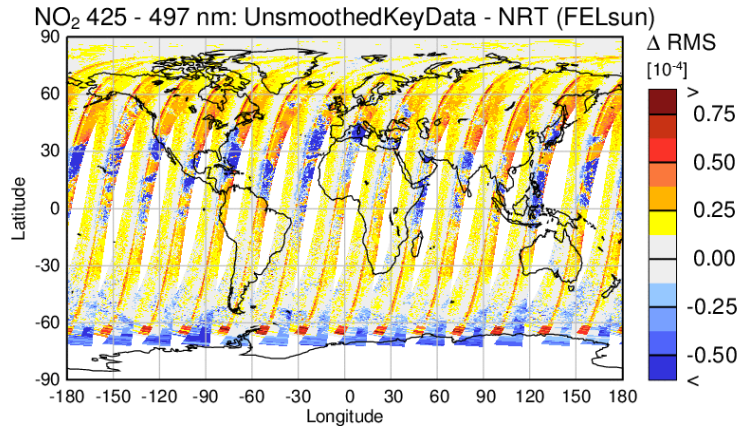


Fig. 37: Difference in RMS of NO<sub>2</sub> retrieval using unsmoothed keydata – NRT data. Red colours indicate better NRT data, blue colours poorer NRT data.

As shown in Fig. 37, smoothing of the keydata improves the fitting quality in the large NO<sub>2</sub> window in most regions as expected. In particular for the centre scan there is a marked improvement relative to the unsmoothed version of the keydata (V1.02). However, there are also some viewing geometries for which the fitting RMS actually deteriorates when applying smoothed keydata, mainly between 0° and 30°N and south of 60°S. This indicates that some of the keydata are improved by the smoothing process while others are getting worse.

#### 6.4 Partial smoothing

In the NRT data set, smoothing is applied in both angular and spectral direction. In order to test if both are needed, two additional data sets have been created starting from keydata V1.02, one where only angular smoothing was applied and another one where angular smoothing and Xe filtering was introduced.

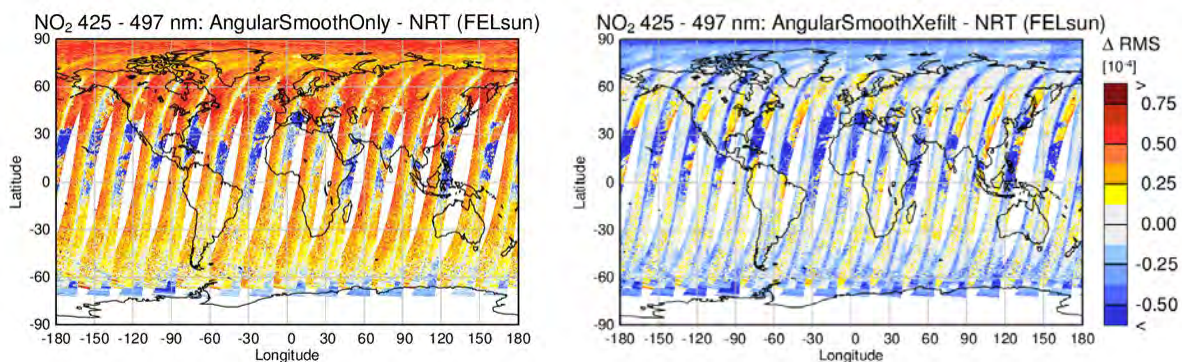


Fig. 38: Difference in RMS of NO<sub>2</sub> retrieval using data where only part of the keydata is smoothed – NRT data. Left: Only angular smoothing has been applied, right: angular smoothing and Xe filtering has been applied. Red colours indicate better NRT data, blue colours poorer NRT data.

As seen in Fig. 38 (left), angular smoothing alone leads to poorer fits than NRT data with the exception of a small latitude region between 0° and 30°N. These are the same regions already highlighted in Fig. 37 for showing better results without smoothing of keydata. If Xe filtering is applied in addition (Fig. 38 right), fitting quality is better than NRT nearly everywhere with small exceptions.

## 6.5 No polarisation correction

The most important calibration for a GOME-type instrument is polarisation correction. In the atmosphere, polarisation depends on scene (surface reflectance, clouds, aerosols), solar position, and viewing direction. In the GOME2 instruments, mainly the scan mirror position and the wavelength determine the polarisation sensitivity. In combination, a systematic geographical pattern of polarisation corrections develops which changes with season.

### 6.5.1 Polarisation correction and NO<sub>2</sub>

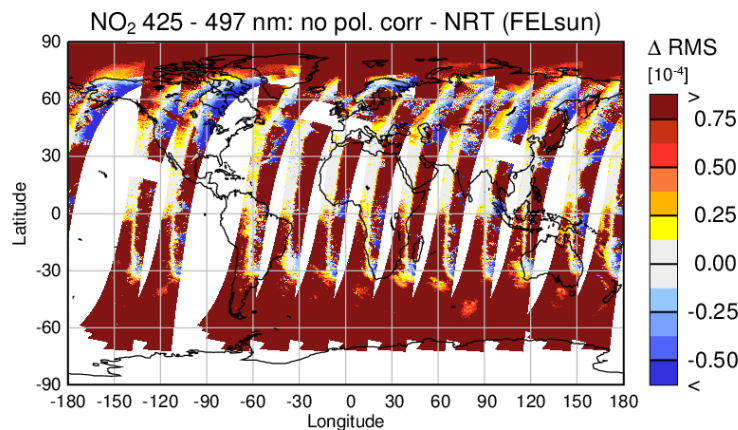


Fig. 39: Difference in RMS of NO<sub>2</sub> retrieval using data without polarisation correction – NRT data. Red colours indicate better NRT data, blue colours poorer NRT data.

As shown in Fig. 39, omitting polarisation correction during calibration results in much poorer fits nearly everywhere as expected. This demonstrates that the polarisation correction in the current processor is already very efficient. However, in some regions fits are clearly better without polarisation correction, indicating that for these situations, the polarisation correction does not work properly. This could be either because of problems in the keydata or because of problems in the computation of the polarisation degree which relies on PMD measurements. As the problem is limited to specific regions and viewing geometries, it appears more plausible that the problem lies with the determination of the degree of polarisation.

## 6.5.2 Polarisation correction and BrO

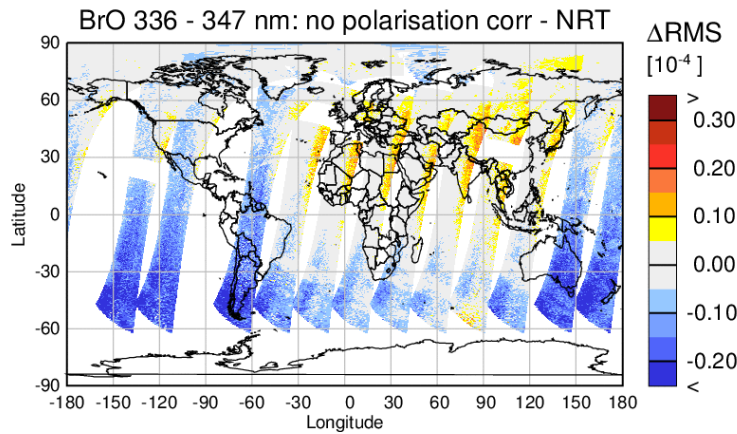


Fig. 40: Difference in RMS of BrO retrieval using data without polarisation correction – NRT data. Red colours indicate better NRT data, blue colours poorer NRT data.

In the BrO fitting window (336 – 347 nm) the polarisation dependency of the GOME2 instruments is weak. In fact, the BrO fitting window has been designed to avoid large polarisation features. Consequently, BrO fitting residuals differ little when comparing data with and without polarisation calibration (Fig. 40).

## 6.5.3 Polarisation correction and OCIO

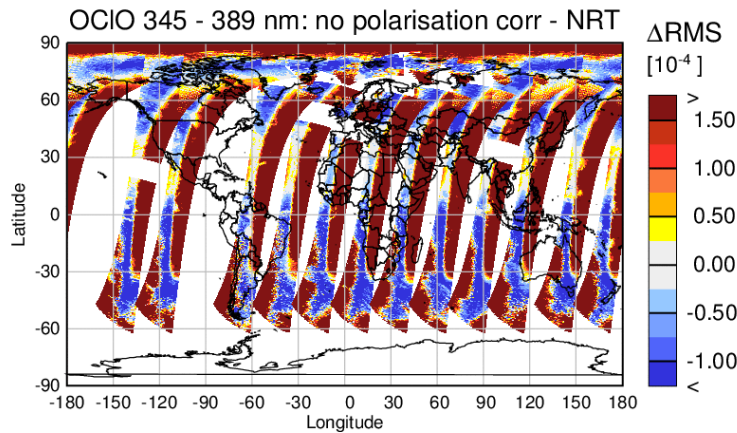


Fig. 41: Difference in RMS of OCIO retrieval using data without polarisation correction – NRT data. Eta has not been included in either of the fits. Red colours indicate better NRT data, blue colours poorer NRT data.

In the OCIO fitting window (345 – 389 nm), the polarisation sensitivity of the GOME2 instruments is large. As OCIO is a weak absorber, proper polarisation correction in this fitting window is important. As shown in Fig. 41, OCIO fits have very low quality over large parts of the orbit when omitting polarisation calibration. However, there is also a systematic pattern of regions where fits actually improve without polarisation calibration.

This indicates that polarisation correction is not always working as expected in this spectral range.

As incomplete polarisation correction has a negative impact on the quality of the retrieved OCIO columns, the eta nadir keydata are often introduced in the retrieval as an additional cross-section. In Fig. 42, the effect of introducing eta in the fit is shown for two cases – one, where eta is used in both fits (left) and one, where eta is only used on the uncorrected data.

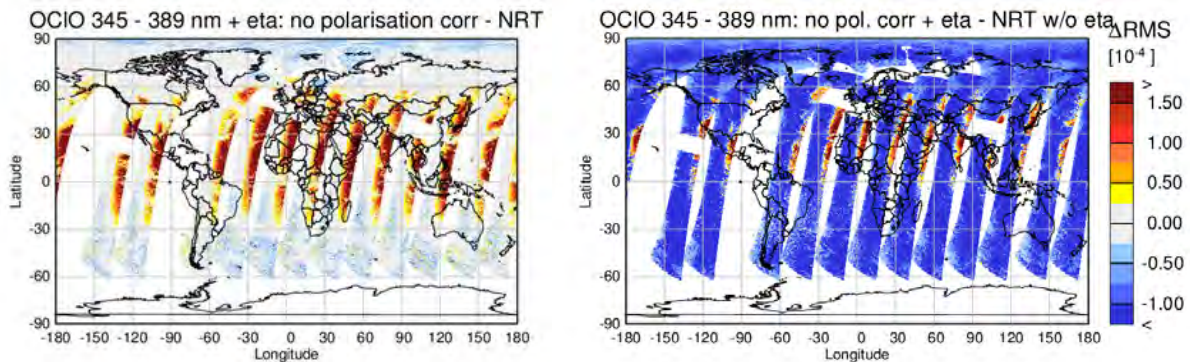


Fig. 42: Difference in RMS of OCIO retrieval using data without polarisation correction – NRT data. Left: eta has been included in both fits, right: eta correction has been included only in the fit on data without polarisation correction. Red colours indicate better NRT data, blue colours poorer NRT data

As can be seen from Fig. 42, eta can compensate for most of the polarisation dependency of the data with the exception of a crescent shaped region on the right side of the orbits which appears to be linked to the largest negative values of  $q$  (compare Fig. 43). In the rest of the orbit, using just eta fitting on not polarisation corrected data results in better fits than using polarisation corrected lv1 data and not including eta in the fit. It is interesting to note that including eta in fits on polarisation corrected data also removes most of the problems in those areas, where polarisation correction deteriorated the fitting quality in Fig. 42.

In summary, polarisation correction is very important in the OCIO retrieval window. The operational correction improves fits in many but not all parts of the orbit. Use of eta as an additional absorber solves many of the problems and in combination with polarisation corrected lv1 data yields the best fits.

## 6.6 Threshold in polarisation correction

Considering the results and conclusions from the previous sections, one possible approach to improve the polarisation correction is to limit its application to regions where it is considered to be reliable. Unstable polarisation calibration can be expected for very low values of  $q$ , and therefore a threshold of  $q > 0.05$  was introduced to avoid applying polarisation correction where no good polarisation measurement is available. As an example, polarisation fractions are shown for one GOME2-B orbit in Fig. 43.

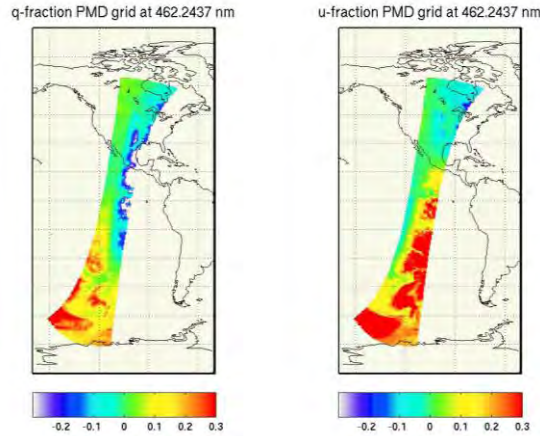


Fig. 43: PMD derived polarisation fractions q (left) and u (right) for one orbit of GOME2-B data

### 6.6.1 Polarisation threshold NO<sub>2</sub>

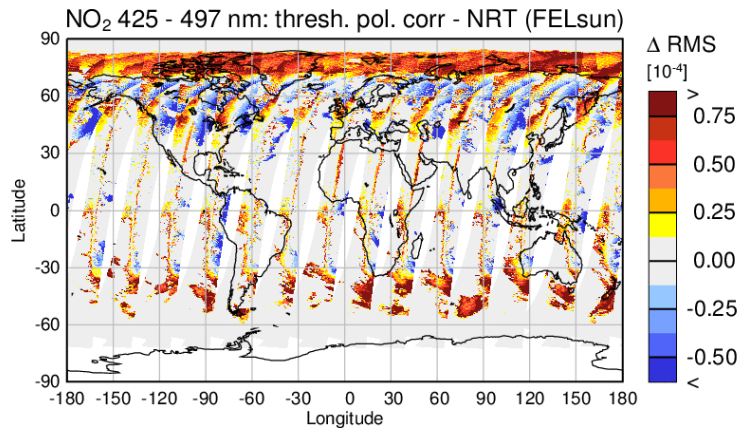


Fig. 44 Difference in RMS of NO<sub>2</sub> retrieval using data where the polarisation correction is limited to regions where  $q > 0.05$  – NRT data. Red colours indicate better NRT data, blue colours poorer NRT data.

As shown in Fig. 44, this approach in deed improves the fitting residuals in some of the regions identified in Fig. 39 without leading to problems in most of the globe. However, there are some fits, in particular at high latitudes but also between 30°N and 60°N where the fitting quality actually deteriorates. It is therefore concluded that a)  $q$  might not be the best quantity to use for selection of regions to exclude polarisation calibration and b) that this selection should not (yet) be implemented in future keydata versions.

### 6.6.2 Polarisation threshold OCIO

A similar conclusion can also be drawn for OCIO. As shown in Fig. 45, some improvements relative to NRT data can be achieved by limiting polarisation correction to scenes having  $q > 0.05$ , but the pattern of low  $q$  does not really match the pattern of poor polarisation correction and thus the effect is not quite as expected.

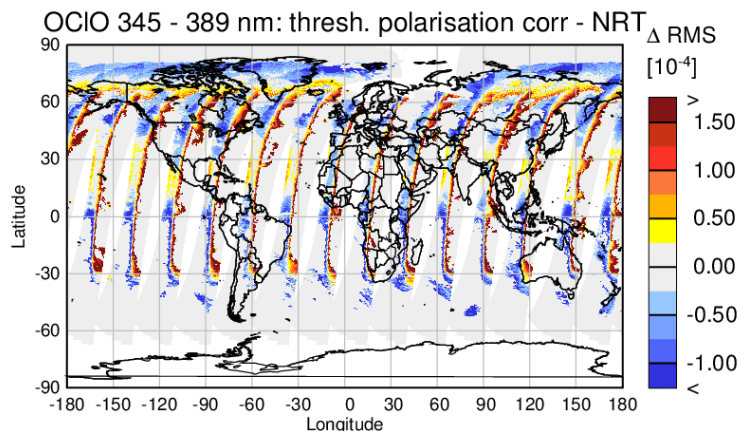


Fig. 45: Difference in RMS of OCIO retrieval using data where the polarisation correction is limited to regions where  $q > 0.05$  – NRT data. Red colours indicate better NRT data, blue colours poorer NRT data.

## 7 Principal Component Analysis (PCA) of fitting residuals

### 7.2 Introduction

#### 7.2.1 Degradation and Calibration - impact on lv2 products

The instrument degradation influences the quality of the lv2 products in the following main aspects:

- A calibration procedure setup relies on the fact that the instrument response does not change over time. The degradation changes the instrument response and thereby influences the evolution of the calibration key data.
- The reduction in throughput can result in loss of information required for accurate calibration e.g. by loss of wavelength calibration lines or PMD signals below a certain intensity threshold.

An improper calibration can have several consequences; it can result in measurements with biases and incomplete correction of spectral features and may introduce artificial structures in the lv0 to lv1 processing as well. The calibration procedure therefore requires continuous monitoring and improvements.

A systematic analysis of the fitting residuals as Principal Component Analysis (PCA) can provide a lead on the deficiencies ensuing from the factors outlined above provided that the systematic structures can be associated with degradation or specific calibration steps which can in turn help to improve on the calibration settings.

### 7.2.2 Principal Component Analysis (PCA)

The Principal Component Analysis is a non parametric linear algebraic technique to extract relevant information from the data by reducing its dimensionality into few variables. This is achieved by using an orthogonal transformation to convert possibly correlated variables into a set of values of linearly uncorrelated variables called principal components that identify the principal directions in which the data varies. The first component accounts for the highest variance in the data and each next component progressively displays smaller variance that was not accounted by the previous.

Statistically, the simple way to compute the principal components is by finding the Eigenvectors (principal directions) and Eigenvalues (principal values) of the covariance matrix which means finding the transform where the covariance matrix is diagonal. The first few components with the highest variance are retained for interpretation. The limitations of PCA lie in the assumptions of linearity in the data and dependence on variances yet it is a power tool for the identification of patterns and outliers in the data which is our objective in his study.

In this work, the software for reading the data, subsets regrouping, analysis and graphical representation is written in IDL. The software uses the IDL built in function 'pcomp' that conducts PCA through the computation of Eigenvectors and the Eigenvalues of the covariance matrix.

### 7.3 Analysis strategy

The PCA of the fitting residuals is experimented to provide answers to the following main questions:

1. Is it possible to identify the degradation effects, instrument issues or calibration deficiencies by PCA?
2. Can we use the information obtained from the analysis to improve on the calibration of spectra?

As inherently PCA is a form of unsupervised learning, the questions at hand should ideally be addressed by studying the residuals of lv2 products from different fitting windows, for longer time periods and comparison of results for several alternate processing parameters and calibration settings to enable investigation of well representative samples and in order to segregate and identify the issues and their effects on residuals. Consequently, the principal components from one test may be used as predictor for the choice of variables in subsequent analyses. The calibration issues may exhibit viewing angle/line of sight (LOS), solar zenith angle (SZA), azimuth angle dependencies so these also have to be taken into account during the course of analysis. Additionally, the resulting Principle Components (PCs) with the highest variances can be tested in the DOAS fit facilitating a better identification and understanding of the

captured signals. While this should be a separate extensive study on its own, here, as a first experiment in this direction, the PCA is conducted on a small subset of data with a selection of case studies as will be shown in the following sections. For the interpretation of PCA results, “a visual inspection of the principal components or Eigenvectors (EVs)” and “comparison to the known calibration issues” is intended here.

## 7.4 Case studies

### 7.4.1 PCA of NO<sub>2</sub> fitting residuals

#### 7.4.1.1 Data Selection

PCA is applied on the NO<sub>2</sub> residuals (channel 3) for the large fitting window, 425 – 497nm, this region is chosen because it still shows problems as outlined in the previous section 4. The residuals are analyzed for four selected days from GOME2-B and, two days of GOME2-A for comparison as:

**GOME2-B:** Jan. 1<sup>st</sup>, 2013, Jul. 1<sup>st</sup> 2013, Jan 1<sup>st</sup>, 2014 and Jul 1<sup>st</sup> 2014

**GOME2-A:** Jan. 1<sup>st</sup> 2008 and Jul. 1<sup>st</sup> 2007

The January and July values are selected to see if seasonal effects are present.

To retain maximum information in the residuals originating from the calibration related issues, following procedure is applied during the retrieval:

- No eta or other soft calibrations are implemented in the retrieval
- No correction of sand structures is performed and
- A low order polynomial is used.

In addition, a South Atlantic Anomaly (SAA) filter is applied on the resulting residuals to remove possible SAA related spikes that may affect the interpretability of the analysis.

#### 7.4.1.2 Eigenvectors inspection

Fig. 46 shows the results of the PCA application on the residuals for the selected days for both instruments. The upper two panels, on the left and right side, depict the Eigenvalues plotted for each component, for the January and July values respectively. As can clearly be seen, the first 4 or 5 Eigenvalues account for most of the variance in the data. The second panel shows the residual means for the respective days. The first five Eigenvectors (EVs) or principal components are displayed in the successive panels.

**Eigenvector 1 (EV1):** The basic spectral shape of EV1 is same on the given days for both instruments. For GOME2-B, EV1s contain higher frequencies for the first year (Jan. and Jul. 2013) compared to those of its second year (Jan. and Jul. 2014), and both years of GOME2-A which are interestingly, smoother and identical to each other. When EV1 of GOME2-B is included in DOAS fit, shown in Fig. 47a, tested and plotted for 1<sup>st</sup> Jan. 2013, it shows a hemispheric gradient with similarities to that as reported before for

the resolution correction for the large NO<sub>2</sub> fitting window (see section 4.4). Some link to the desert regions is also observable here. Note that the sand structure correction was not included in the retrieval.

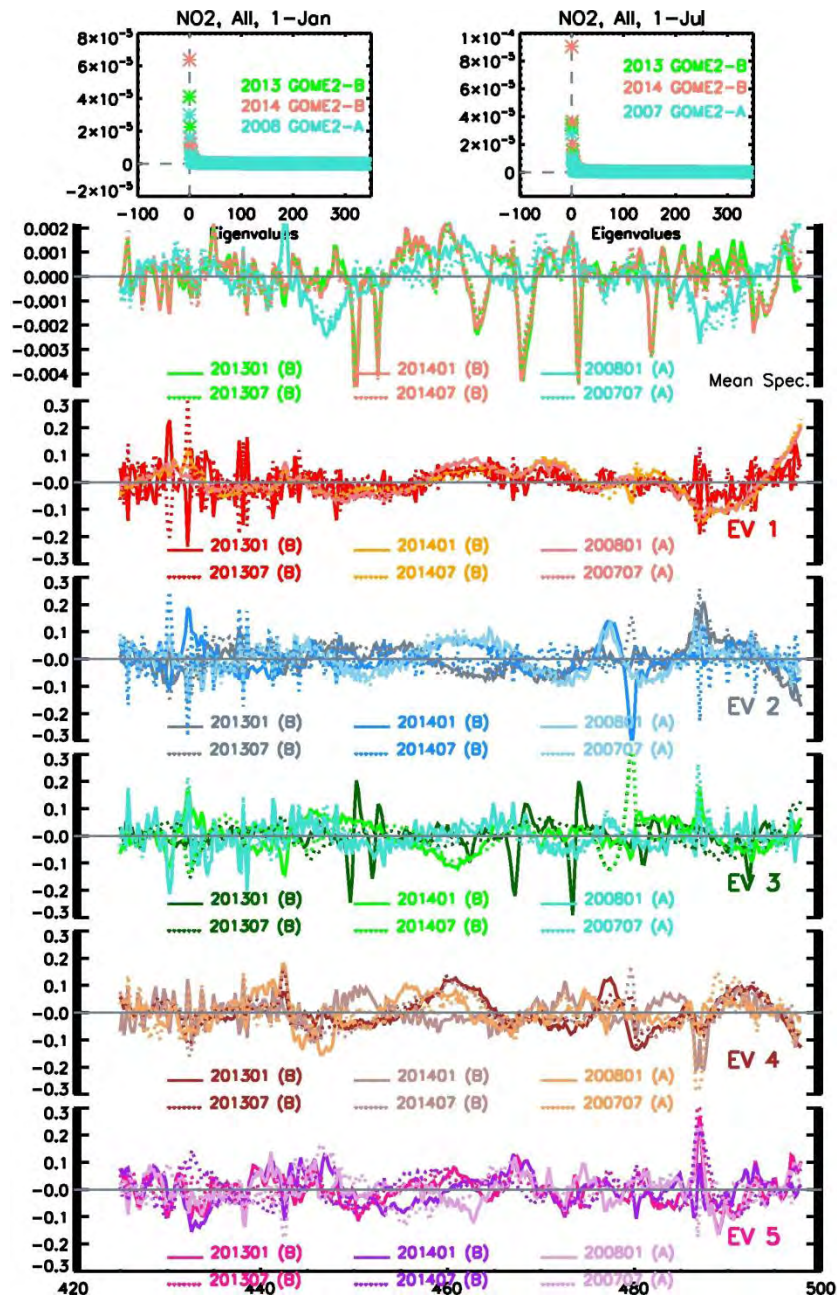


Fig. 46: PCA results for the GOME2-A and GOME2-B NO<sub>2</sub> residuals in the large fitting window (425 -495 nm, x-axis) for the selected days. The upper small panels show the Eigenvalues for 1<sup>st</sup> Jan. and 1<sup>st</sup> Jul. values for the studied years on the left and right side respectively. The next panel shows the associated mean residuals. The subsequent panels display the first five Eigenvectors (EVs).

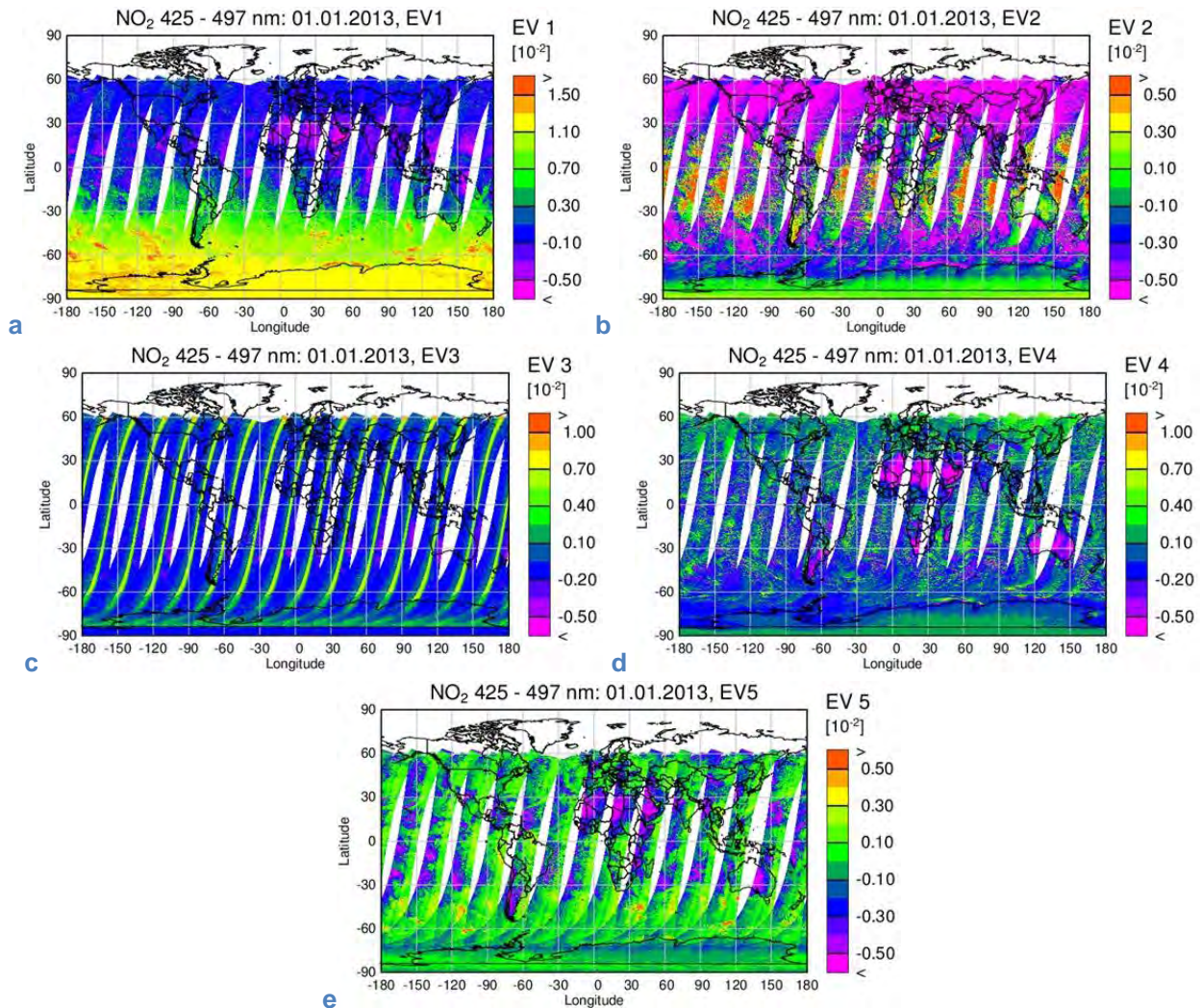


Fig. 47: The DOAS fit result for the Eigenvectors EV1, EV2, EV3, EV4 and EV5 of Fig. 46

**Eigenvector 2 (EV2):** EV2 exhibits some similarities as well as differences among the considered days for both instruments. It appears to mirror some structures of EV1 e.g. for GOME2-B, the peaks observe around 430 and 486nm. Inclusion of this vector in the DOAS fit, performed here for GOME2-B, 1<sup>st</sup> Jan. 2013 and presented in Fig. 47b, highlights the right part of the orbits which is a known region where polarisation correction is most important for the NO<sub>2</sub> large fitting window (See Sec. 4.3). Negative values at high latitudes are also noticeable but cannot be explained easily as these could result from a mixture of different effects.

**Eigenvector 3 (EV3):** EV3 for 1<sup>st</sup> Jan. 2013 for GOME2-B is considerably different from the rest of chosen days of GOME2-B as well as those of GOME2-A, containing spiky structures similar to known Xenon peaks issue of the key data. Keeping in view that the other selected days of GOME2-B fall after May 2013, when the key data was updated and cleaned from the spurious structure, the disappearance of the lines for these days

can be potentially linked to the key data cleaning. Inclusion of EV3 for 1<sup>st</sup> Jan. 2013 for GOME2-B in the DOAS fit, depicted in Fig. 47c, gives high values for the well-known 9 – 11 subsets problem with xenon spectral lines in the key data.

**Eigenvector 4 (EV4):** EV4 is smoother compared to the previous EVs from both instruments. Especially for GOME2-B, the spectral structure clearly resembles the desert signature which was not corrected in the fit. Incorporating EV4 in the DOAS fit for GOME2-B, 1<sup>st</sup> Jan. 2013 (Fig. 47d) indeed shows negative values for the desert regions implying the presence of sand structure signals.

**Eigenvector 5 (EV5):** EV5 is has intermediate frequency for all selected days and appears to be more of a mixture of previous EVs. Fitting this in DOAS for GOME2-B, 1<sup>st</sup> Jan. 2013, presented in Fig. 47e, gives largest values for the right side of the orbit and shows some connection with the dessert signals.

#### *7.4.1.3 Analysis by latitudinal division:*

As some calibration parameters, e.g. polarization fractions, can exhibit latitudinal dependencies, the NO<sub>2</sub> residuals studied above are analyzed for three subsets of latitude divisions, the northern hemisphere (30°N -90°N), southern hemisphere (30°S-90°S) and the tropics (30°N-30°S). Similar to Fig. 46, the PCA results for the north and south are shown here in Fig. 48a and Fig. 48b respectively. For the tropics, see App. A1.

EV1 is nearly identical for the instruments in all hemispheres (consequently the seasons) and in time periods with the exception of some features for 1<sup>st</sup> Jan. 2013, GOME2-B. Compared to the previous analysis (Fig. 46), here the shape of EV1 is visually evident to have remarkable similarities with the NO<sub>2</sub> residual spectrum of east and west scans (see sec 3.4, Fig. 14) which demonstrated systematic, smooth differences in the scans linked to the scan angle dependent degradation. EV2, EV3 and EV4 show similarities as well as differences among each other in addition to some change of order for the hemispheres. This indicates the presence of atmospheric or surface features in the EVs. A striking attribute are the Xenon lines which again only appear before the key data update, in EV2 for north, EV3 in the south, and EV4 in the tropics adding to our previous conclusion. Moreover, for all hemispheres, a spike is seen in EV2 around 480nm in GOME2-B only after the key data cleaning indicating that the update possibly introduced some features in addition to removing spurious lines. EV4 and EV5 for the southern hemisphere show a strange peak around 458 nm in GOME2-B that only appears in 1<sup>st</sup> Jan, 2014 and cannot be explained at this point.

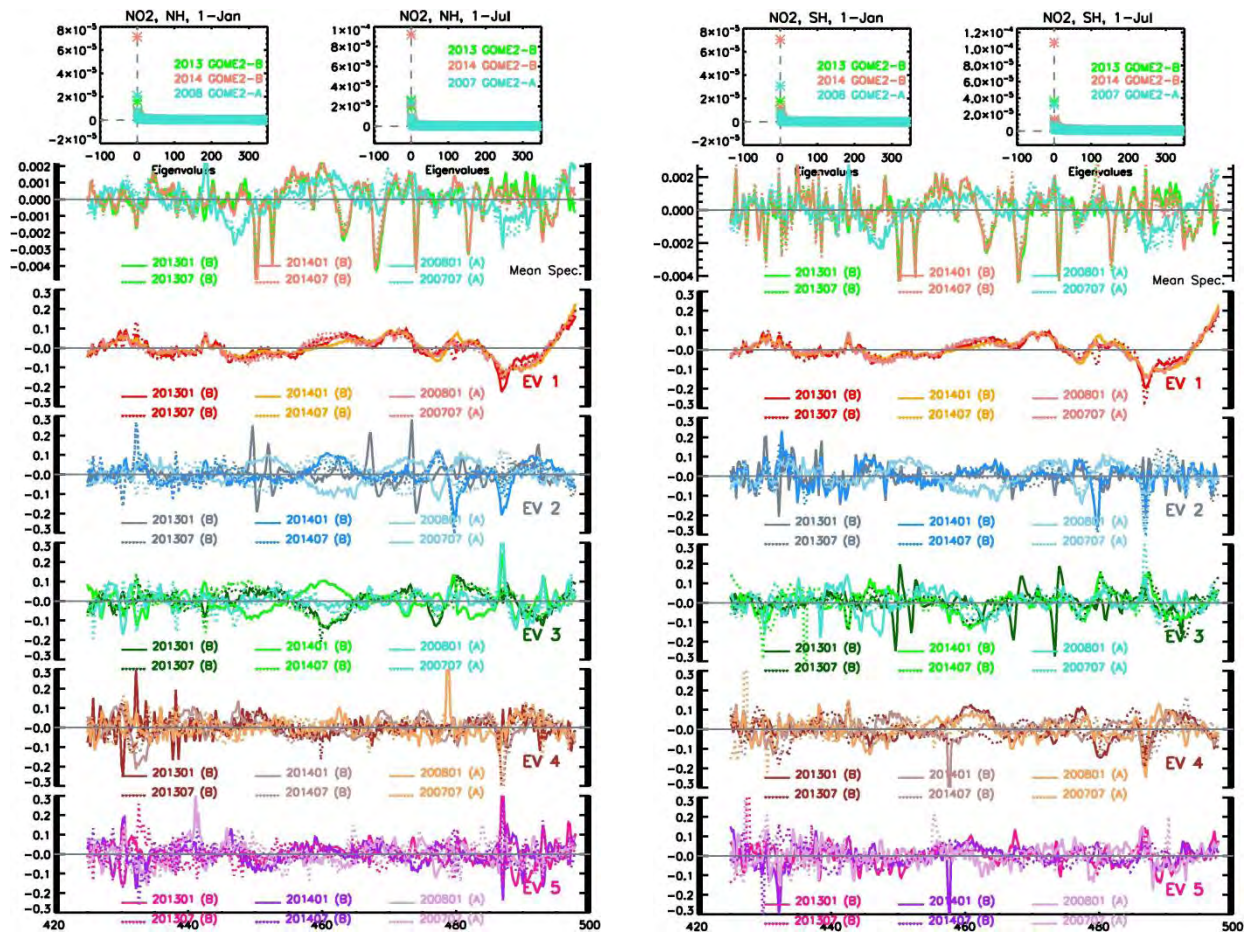


Fig. 48: Similar to Fig. 46 but PCA results for the GOME2-A and GOME2-B NO<sub>2</sub> residuals (425-495nm, x-axis) for the 1<sup>st</sup> Jan. and 1<sup>st</sup> Jul. values for the northern (a) and southern (b) hemispheric subsets on left and right respectively.

#### 7.4.1.4 Analysis of viewing angle dependency:

The NO<sub>2</sub> residuals are also analyzed for the viewing angle/LOS dependence of the calibration deficiencies. Fig. 49a-c depict the PCA results for GOME2-B, 1<sup>st</sup> Jan. 2013 and 1<sup>st</sup> Jan. 2014 and for GOME2-A, 1<sup>st</sup> Jan. 2008 respectively for 9 subsets separated by LOS. Analyses for the rest of the days are included in App. A2.

No clear LOS dependency is observed on any of the studied days. Before the key data update, for all LOS subsets the GOME2-B EV1 are identical (Fig. 48a), the days afterwards (Fig. 48b and App. A2) show some differences for the subset -35 - -45, i.e. the most eastern side indicating possible introduction of issues with this subset by the update which means one or more calibration steps need improvement. The EV1 for GOME2-A are smoother compared to GOME2-B (Fig. 48c and App. A2). EV2 to EV5 have similarities as well as differences among all days of GOME2-B. As is clear from Fig. 48a, the LOS -25 -- -15 for 1<sup>st</sup> Jan. 2013 shows a peak around 490 nm in EV2 and EV3, and, Xenon lines in EV5, not observed in the later days. On the other hand the

days studied after 1<sup>st</sup> Jan. 2013 show a peak around 480 nm for all LOS, in several EVs of any day, this observation confirms the previous conclusion about introduction of this peak by the key data cleaning. The dubious peaks observed in the south on 1<sup>st</sup> Jan. 2014 around 480nm, can be identified in EV3 and EV4 for the 25 – 35 subset.

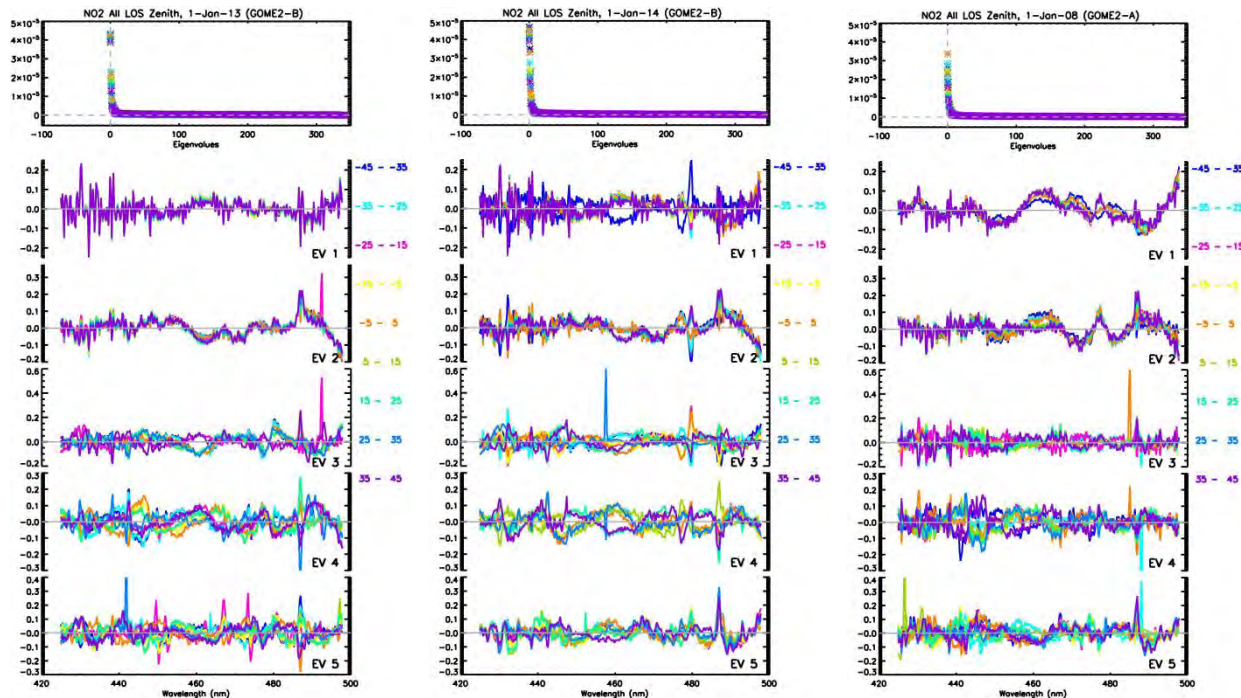


Fig. 49: PCA results for NO<sub>2</sub> residuals (425-495nm, x-axis) for the GOME2-B (1<sup>st</sup> Jan. 2013 on left (22a) and 1<sup>st</sup> Jan. 2014 in the center (22b)) and GOME2-A (1<sup>st</sup> Jan. 2008 on right (22c)) values for 9 LOS subsets. In each figure, the upper panels display the Eigenvalues, the subsequent panels depict the first five Eigenvectors.

## 7.4.2 PCA of new dataset with improved key data

PCA is also applied on the new dataset for particular cases with improved calibrations for impact evaluation study. The residuals are analysed for GOME2-B on a reference day of 24<sup>th</sup> April, 2014 for the NO<sub>2</sub> large fitting window. The following calibration sets are investigated (see Table 3):

### K5\_K8

NRT data with improved FEL calibrated solar background spectrum

### K9

Angular smoothed only data with improved FEL calibrated solar background spectrum

### K10

Angular smoothed only data with Xenon filter and improved FEL calibrated solar background spectrum

It should be noted that a higher order polynomial is used in the DOAS fit for all three test cases listed above.

The analysis is carried out on subsets divided by latitudes and LOS as performed before.

#### 7.4.2.1 Analysis by latitudinal division:

The PCA results are shown here for the northern and southern hemispheres in Fig. 50a and Fig. 50b respectively. For the tropics see App. A3. In all cases, the mean spectra are quite similar with the exception of some peaks around 450 and 470 nm in K9.

The EVs corresponding to K9 and K10 are almost identical in all regions. The Xenon filter does not seem to bring any visible change when the combination of angular smoothing and FEL solar background is used.

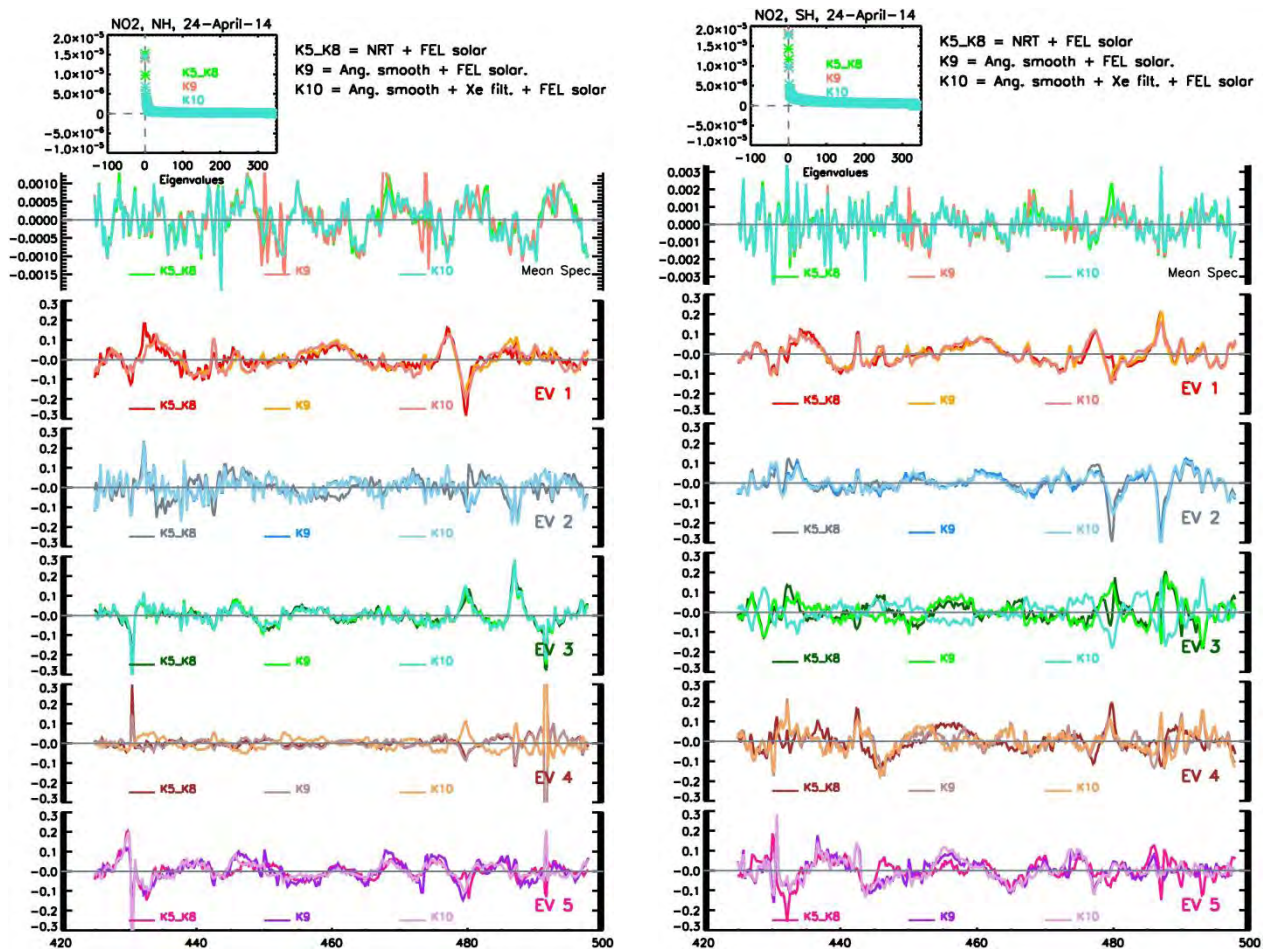


Fig. 50: Similar to Fig. 46 but for the improved keydata combinations K5\_K8, K9 and K10 for the northern (a) and southern (b) hemispheric subsets on left and right respectively

### 7.4.2.2 Analysis of viewing angle dependency:

No clear LOS dependency is observed (Fig. 51a-c). All EVs of K9 are identical to those of K10. For K5\_K8, EV1 for the most eastern subsets, -45 - -35 shows some differences compared to the other LOS subsets (Fig. 51a) hinting at issues with this part of the scan. This difference disappears in EV1 of K9 and K10 implying that the angular smoothing is doing a good work. Few large spikes are present in all calibration combinations, e.g. in EV2 for 5 – 15 subset around 490 nm and EV5 for -25 -15 close to 438 nm.

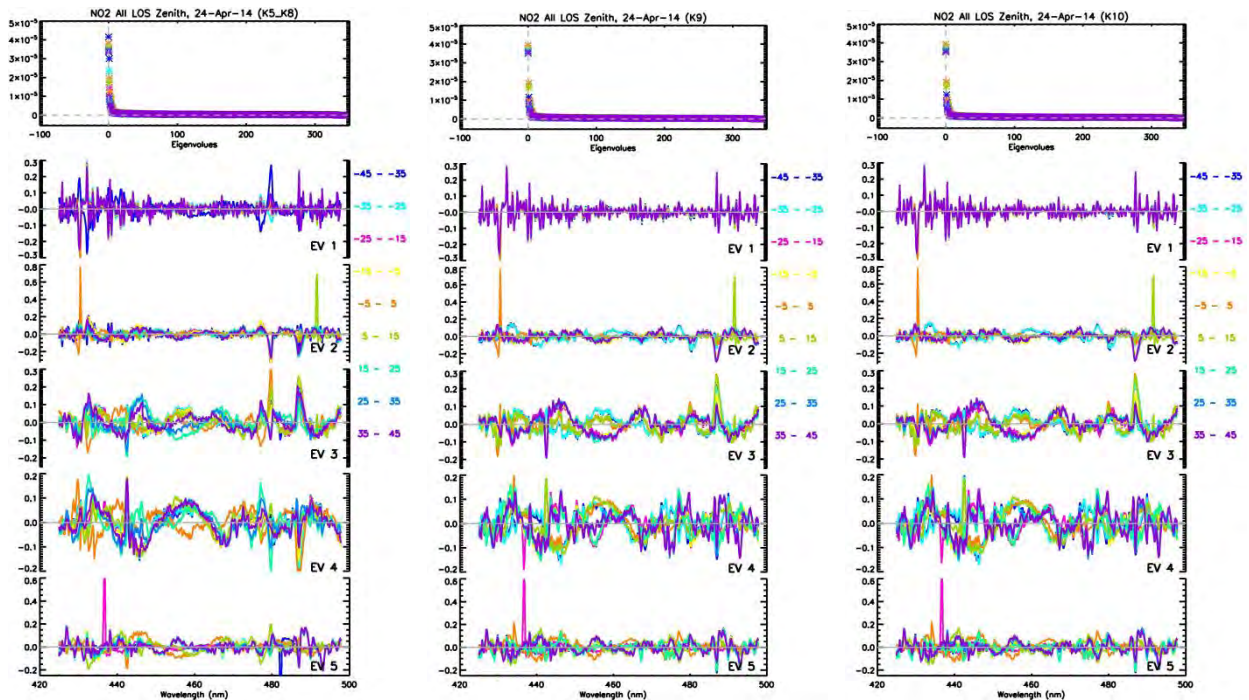


Fig. 51: Similar to Fig. 48 but for NO<sub>2</sub> residuals of GOME2-B with the improved keydata, K5\_K8 (a, left), K9 (b, center) and K10 (c, right) for the 9 LOS subsets.

### 7.4.3 Impact of no polarization correction

The impact of polarization correction being turned off on the fit residuals is analysed on the NRT data with FEL calibrated solar background spectrum and without polarization calibration, namely **K4\_K8** and the results are compared with K5\_K8.

Again the latitude and LOS subsets are examined.

#### 7.4.3.1 Analysis by latitudinal division:

The mean residuals of the regions are different from each other. For the north, the mean residuals are similar for K5\_K8 and K4\_K8 (Fig. 52a), differences appear in the south (Fig. 52b) and the tropics (App. A4) where the amplitude of the K4\_K8 residuals is large.

In all regions, EV1 and EV4 are similar for FEL+ no polarization vs NRT+FEL and contain eta type frequencies. The rest of EVs show differences in spectral shapes and/or

frequencies for both cases as well as similarities among each other implying the presence of atmospheric or surface effects. Peaks are observed in several EVs, especially in the northern hemisphere around 430 nm and the spectral segment between 480 and 490 nm in both K5\_K8 and K4\_K8.

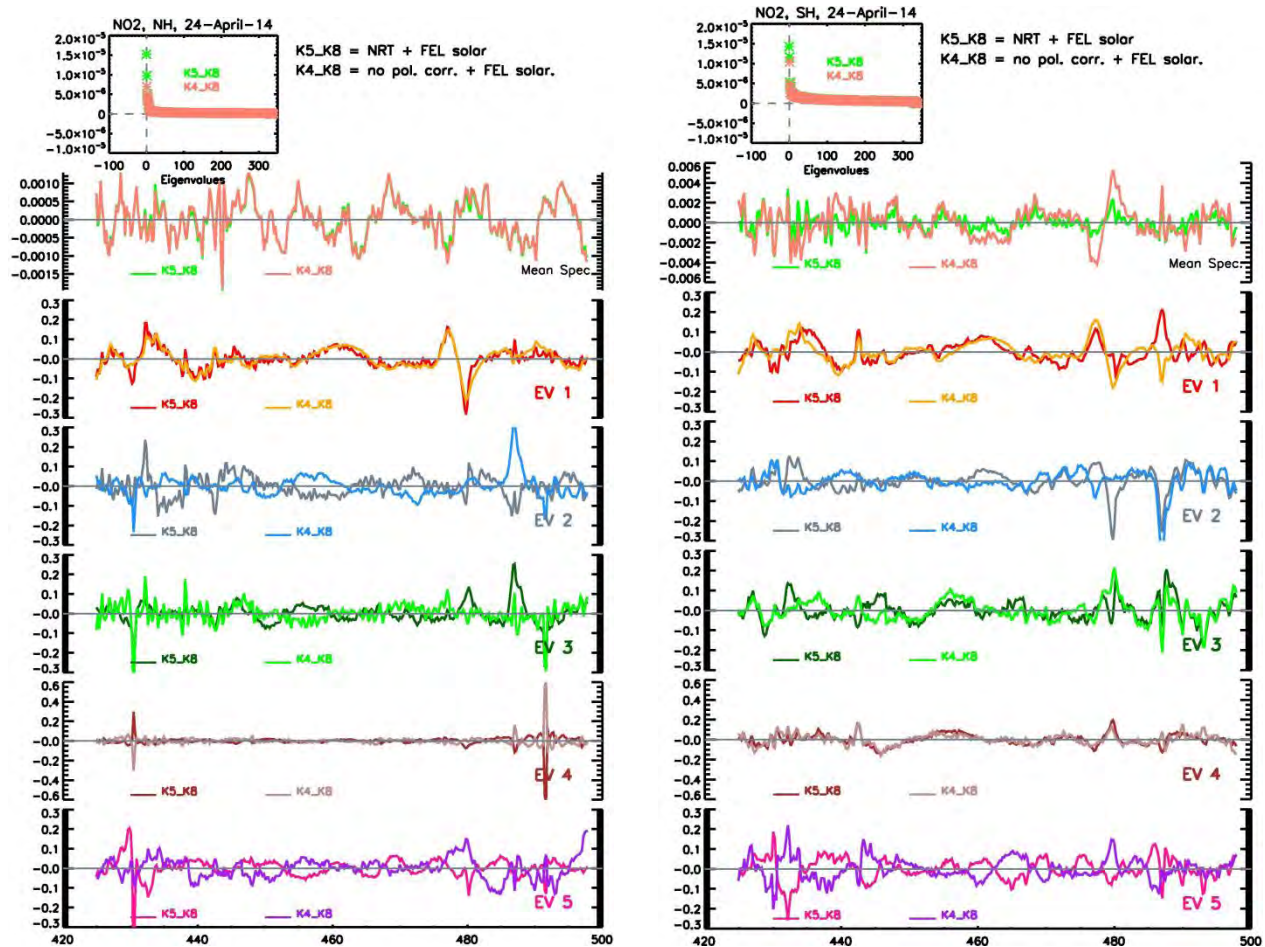


Fig. 52: Similar to Fig. 48 but for the improved keydata combinations for the polarization impact for northern (a) and southern (b) hemispheric subsets on left and right respectively. K4\_K8 is with polarization being turned off, the results are compared to K5\_K8.

#### 7.4.3.2 Analysis of viewing angle dependency:

The EV1 and EV2 of K4\_K8 (Fig. 53) show no evident LOS dependency. EV1 and EV2 are quite identical for all LOS subsets. EV1 here is similar to that for the northern hemisphere. EV2 of K4\_K8 is comparable to EV1 of K5\_K8 (Fig. 51a) containing high frequencies. EV3 to EV5 show some degree of LOS influence, e.g. LOS 5 – 15 is distinguishable from the rest with either very small amplitude or because it contains peak. The spike observed in EV5 for K5\_K8 at -25 -15 (around 438 nm) is also visible here, which means that this feature is not introduced by the polarization correction.

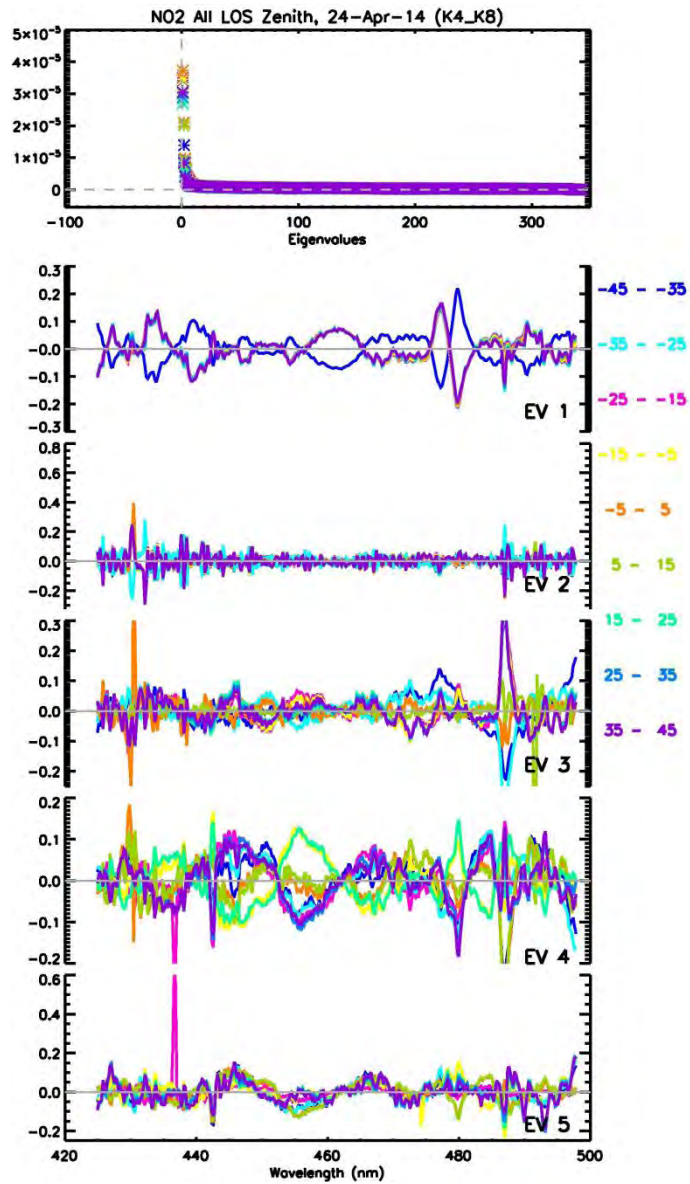


Fig. 53: Similar to Fig xx but for NO<sub>2</sub> residuals of GOME2-B with the improved keydata with polarization calibration turned off, K4\_K8, for the 9 LOS subsets.

#### 7.4.4 Impact of low order polynomial on NO<sub>2</sub>

In the NO<sub>2</sub> large fitting window, a high order polynomial is used to correct for the scan angle dependent degradation. To investigate the relevant deficiencies, the PCA was carried out on two test cases with low order polynomial applied in the fit:

##### K9\_p4

Angular smoothed only data with improved FEL calibrated solar background spectrum and polynomial of degree 4 used in the fit

## K10\_p4

Angular smoothed only data with Xenon filter and improved FEL calibrated solar background spectrum with polynomial of degree 4 used in the fit.

As before, the latitude and LOS subsets are analysed. The results are compared with those of K9 and K10.

### 7.4.4.1 Analysis by latitudinal division:

The mean residuals for the low order polynomial cases, i.e. for K9\_p4 and K10\_p4, of the studied subsets are identical (Fig. 54a and b for north and south respectively and App. A4 for the tropics). The means become large where the amplitude for K9 and K10 is small.

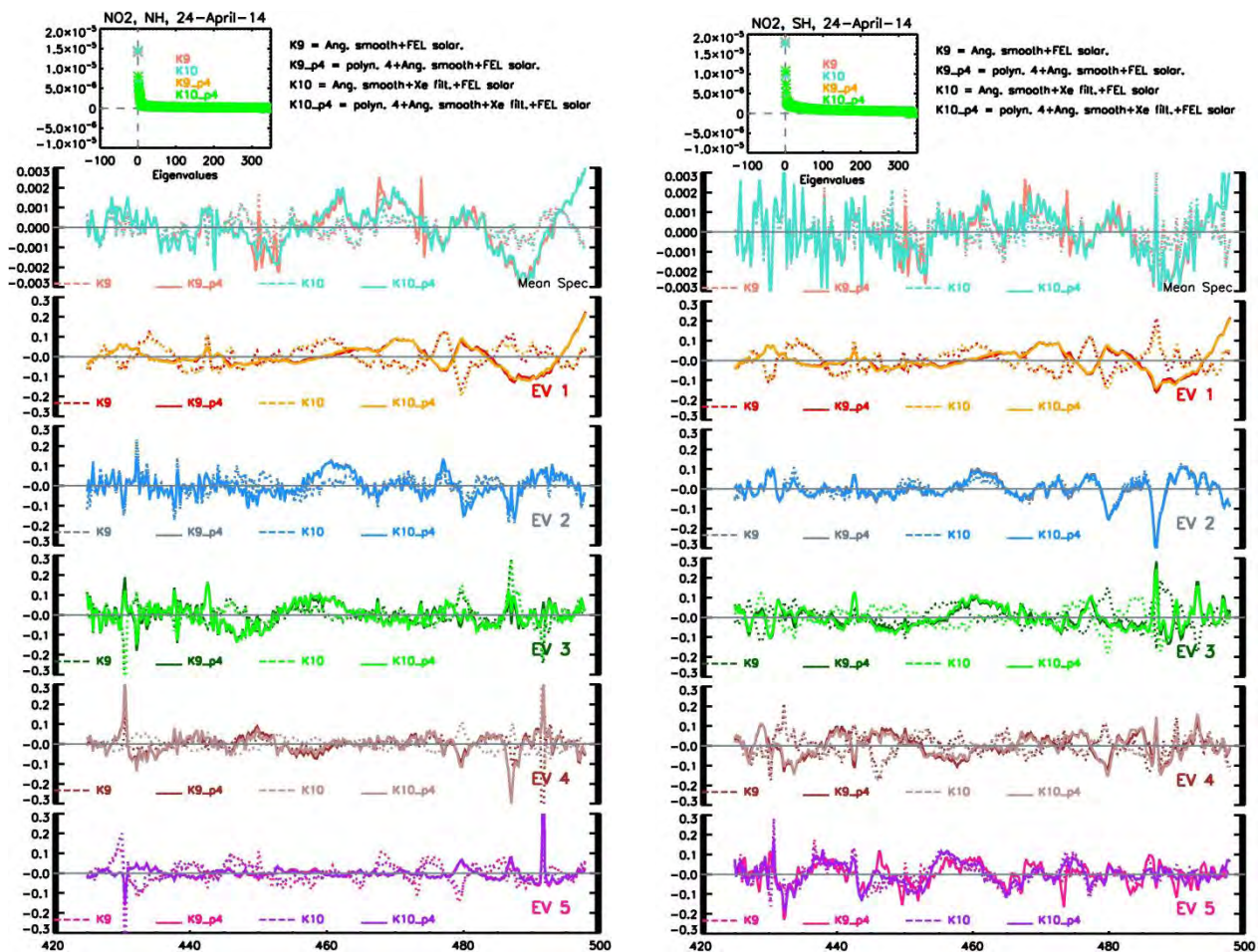


Fig. 54: Similar to Fig. 48 but for the improved keydata combinations for the low order polynomial impact for northern (a) and southern (b) hemispheric subsets on left and right respectively. K9\_p4 and K10\_p4 are with polynomial of degree 4, the results are compared to K9 and K10.

Compared to K9 and K10, the use of low order polynomial in K9\_p4 and K10\_p4 changed the EV1 shape which then resembles the residuals of the difference between

east and west scans adding to the observation that the low order polynomial increases the scan angle dependency (see sec. 3.4). EV2 to EV5 have similarities and differences.

#### 7.4.4.2 Analysis of viewing angle dependency:

The EV1 of K9\_p4 and K10\_p4 are similar for all LOS subsets (Fig. 55a and Fig. 55b). EV3 to EV5 show differences specifically for LOS 5 -15, being very flat for EV3. It remains to be investigated how much this LOS contributes to the east-west scan difference.

In general, the impact of changing the degree of polynomial used in the fit appears to be larger than the polarization correction.

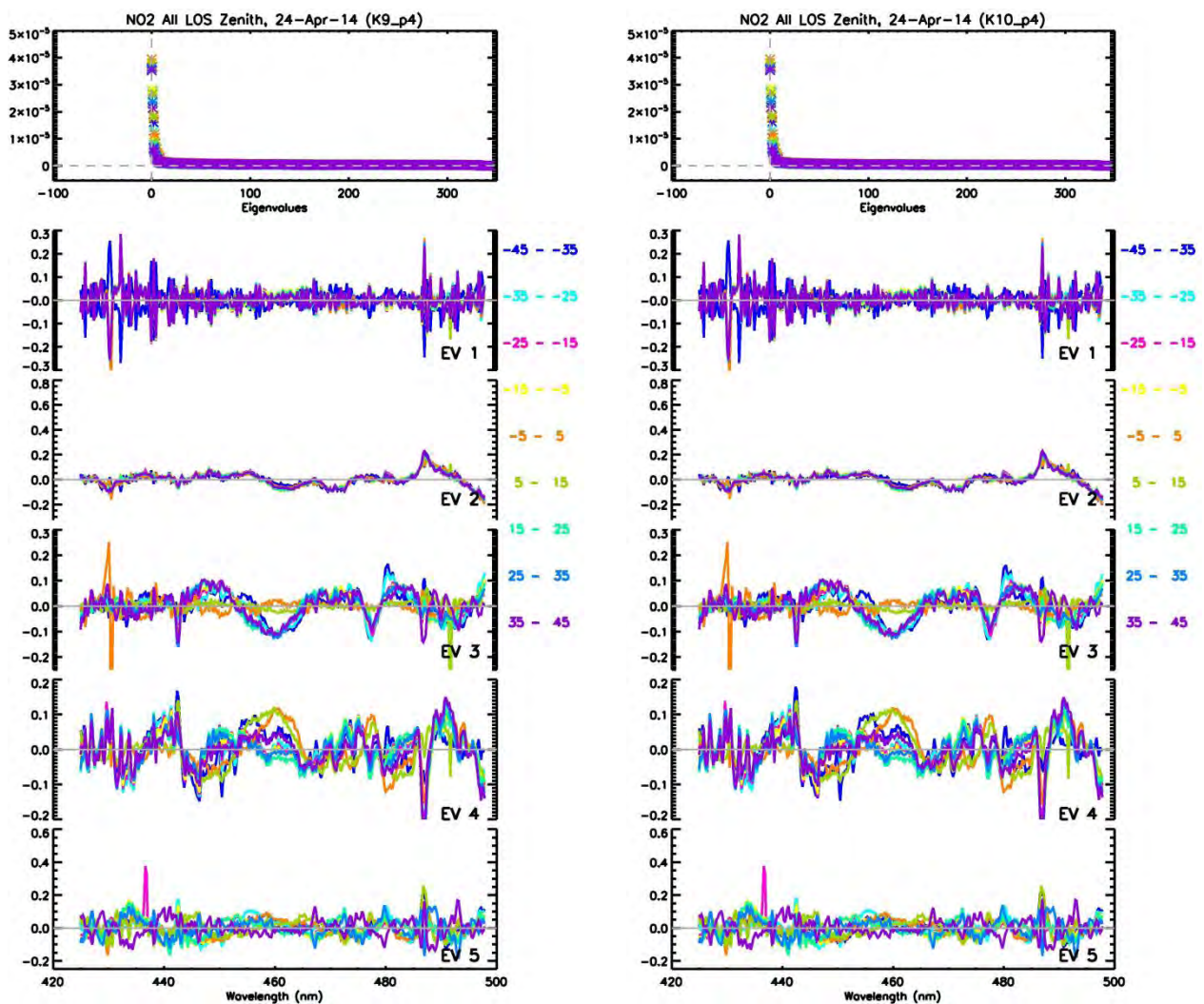


Fig. 55: Similar to Fig. 49 but for NO<sub>2</sub> residuals of GOME2-B with the improved keydata and low order polynomial combinations, K9\_p4 and K10\_p4 for the 9 LOS subsets

### 7.4.5 PCA of OCIO residuals

In channel 2 of GOME2-B, the OCIO residuals (345- 389 nm) are analyzed for a test day 1<sup>st</sup> Jul. 2013. Similar to the NO<sub>2</sub> analyses, the latitudinal and LOS subsets are investigated.

#### 7.4.5.1 Analysis by latitudinal division:

Fig. 56a shows the results for the northern and southern hemispheres as well as the tropics. The mean residuals are very similar for all these regions. Compared to NO<sub>2</sub>, here the EVs show a complicated mixture. EV1 of the northern and southern hemispheres are very similar. EV1, EV2 and EV3 for the north show some spikes around 355 nm and 363 nm not visible in the other subsets.

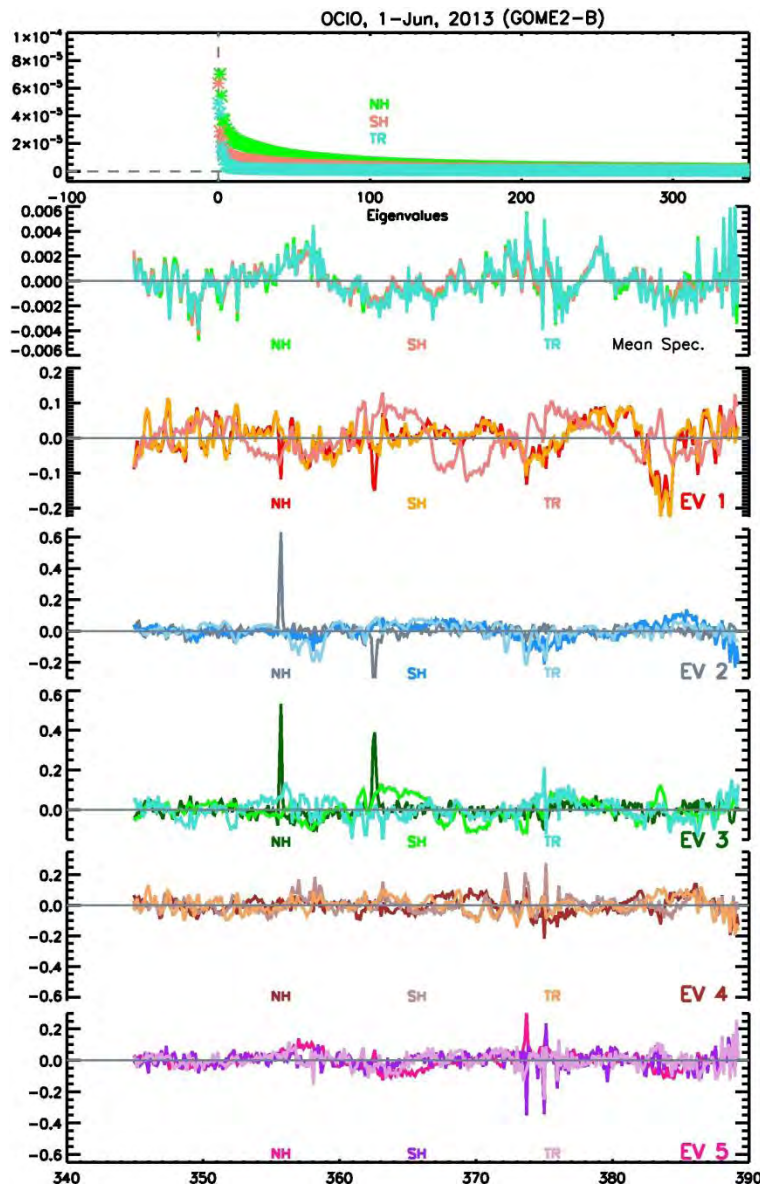


Fig. 56: Similar to Fig. 48 but for the GOME2-B OCIO residuals (345-389 nm, x-axis) for the north south and the tropics subsets.

*Analysis of viewing angle dependency:*

For OCIO, all EVs for the LOS subsets contain very high frequencies (Fig. 57); no conclusion can be drawn from the visual inspection.

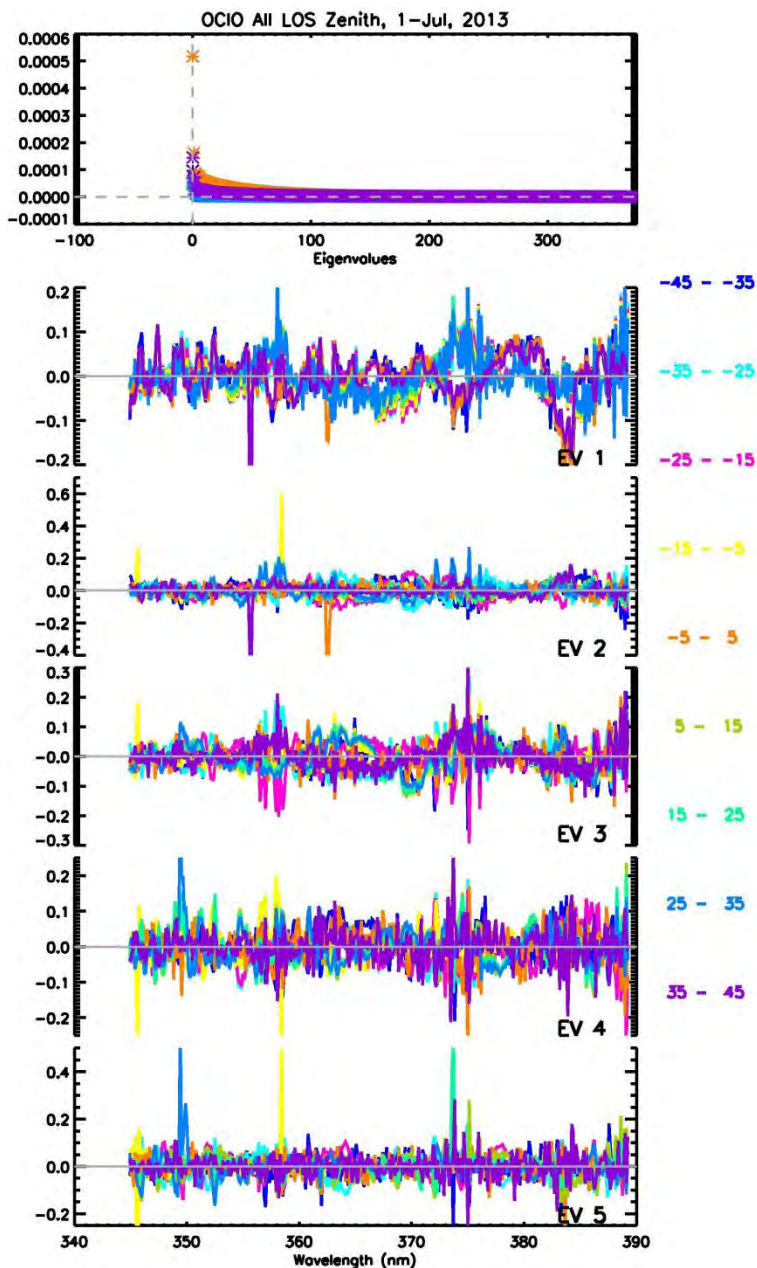


Fig. 57: Similar to Fig. 49 but for OCIO residuals of GOME2-B for the 9 LOS subsets

### 3.3.6 Impact of no polarization correction on OCIO

The OCIO residuals were extracted for the reference day of 24<sup>th</sup> April, 2014 without polarization calibration being applied in the fit and studied for the hemispheric and LOS subsets.

#### 7.4.5.2 Analysis by latitudinal division:

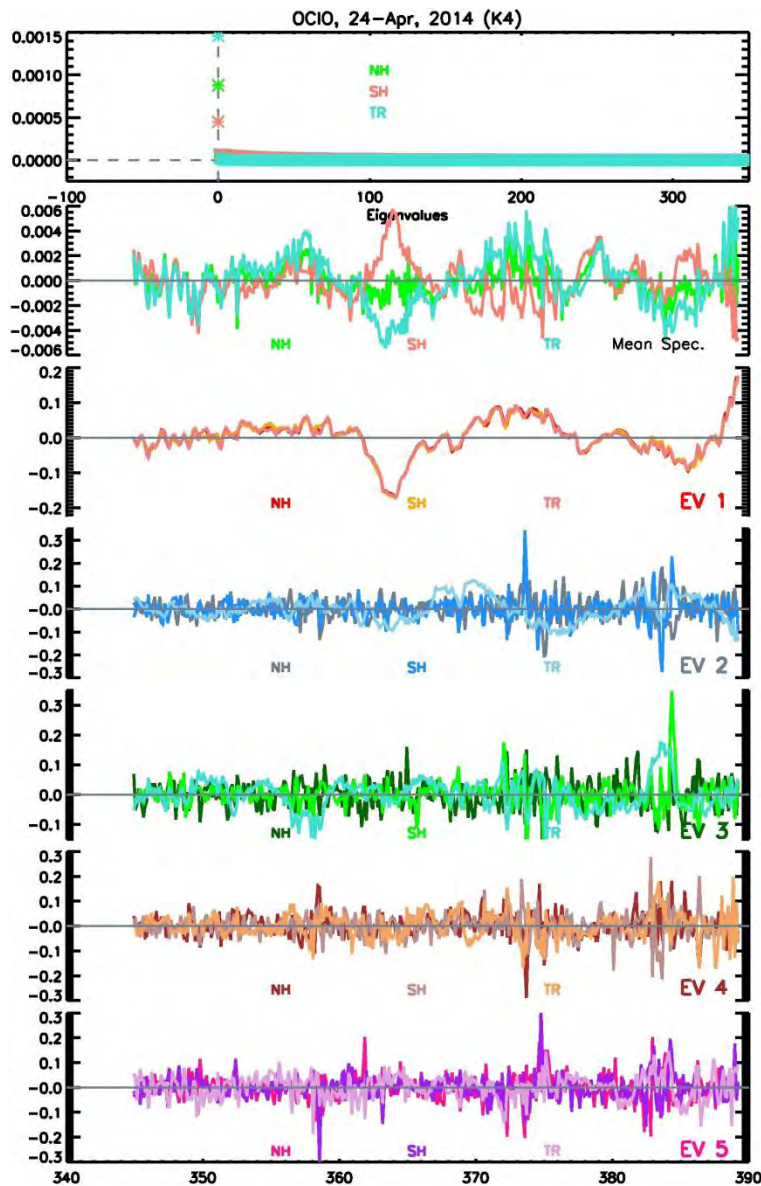


Fig. 58: Similar to Fig. 48 but for the GOME2-B OCIO residuals (345-389 nm, x-axis) without polarization calibration for the north, south and the tropics subsets.

As clear from Fig. 58, without polarization correction, the mean residuals for the south exhibit differences with the rest, which implies that polarization correction may be more

important in the south (summer hemisphere) compared to the other parts. EV1 for all regions is very smooth and identical. The rest of the EVs are very noisy.

#### 7.4.5.3 Analysis of viewing angle dependency:

The EV1 for all LOS (Fig. 59) are interestingly similar and resemble the EV1 for the latitude subsets for this case. EV2 to EV4 are again very high frequency spectra.

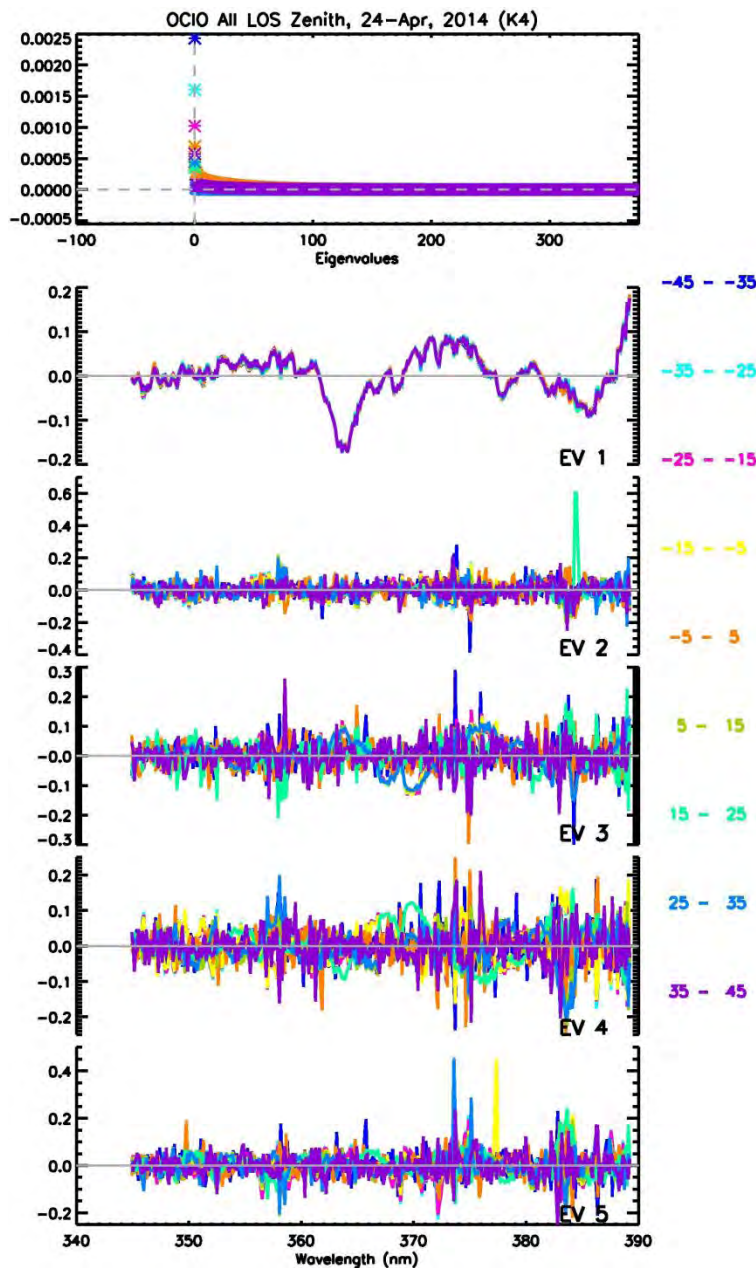


Fig. 59: Similar to Fig xxx but for OCIO residuals of GOME2-B without polarization correction for the 9 LOS subsets

## 7.5 Summary

In this section, a systematic analysis of residuals from GOME2 MetOp-B fits is performed on experimental basis on selected lv2 products, in an attempt to isolate problems in the lv1 data and to find a link with degradation or calibration deficiencies.

In the test cases analysed by PCA, not only some calibration issues but also fitting problems could be identified.

### **NO<sub>2</sub> residuals for the large fitting window:**

- The May 2013 keydata update for GOME2-B smoothed out spurious features such as Xenon lines but also appears to introduce some structures e.g. around 480 nm observed in latitude as well as LOS subsets only for the days after the keydata update.
- Calibrations issues exist around 430 nm and the region between 480-490 nm. This problem has already been linked to the calibration deficiencies in the previous studies.
- The scan angle dependent degradation is dominant in channel 3, both in GOME2-B and GOME2-A as demonstrated by the shape of EV1 for the latitude and LOS divisions which matches the residuals for the east and west pixels.
- Calibration deficiencies still remain for the most eastern part of the scan i.e. LOS -35 - -45.

### **NO<sub>2</sub> residuals for the new key data:**

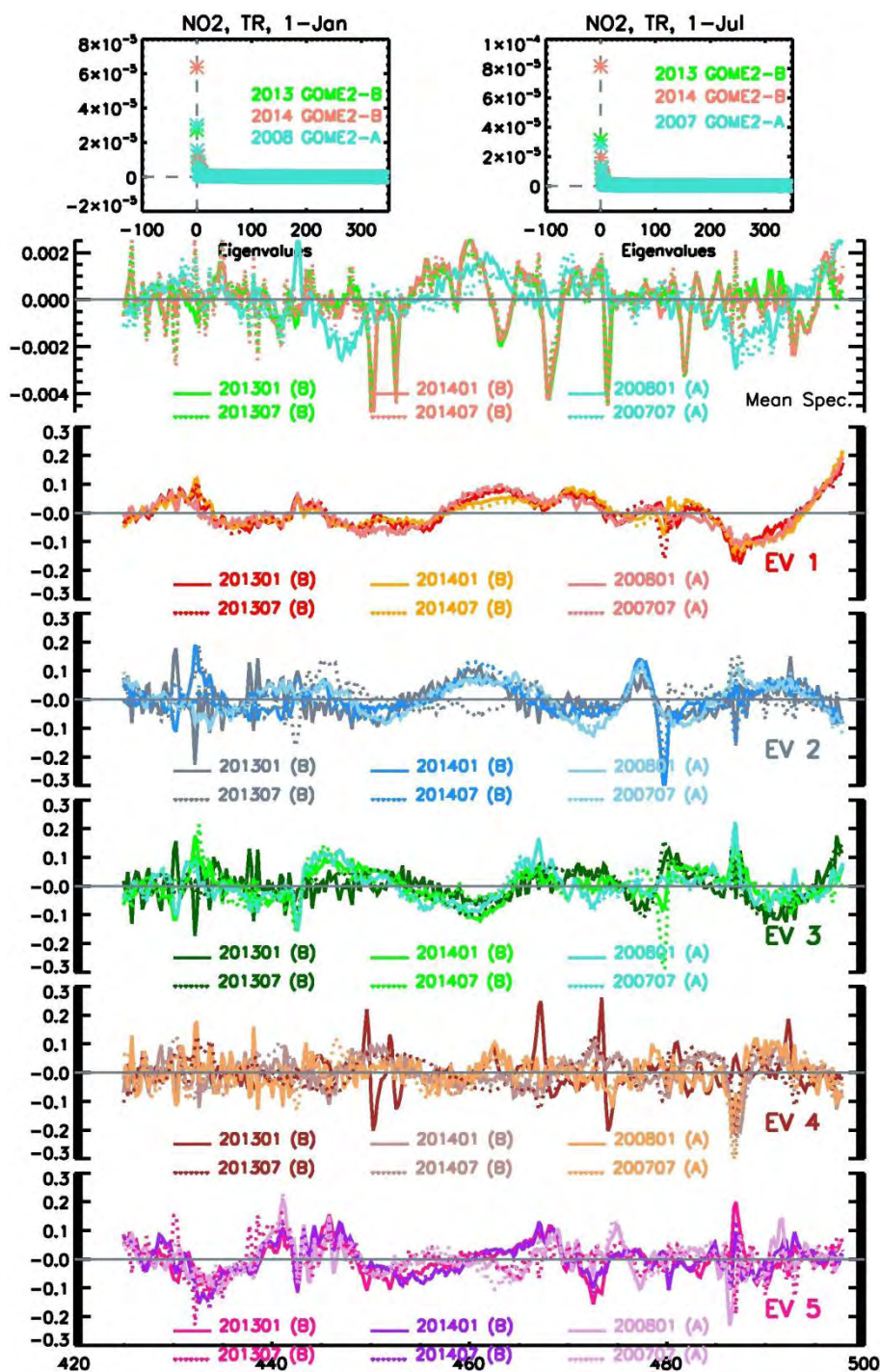
- The FEL calibration with angular smoothing is sufficient as Xenon filter applied in addition shows no change in the residuals or the EVs. This combination seems to deal with the issues with the most eastern scans -35 - -45 to some extent. The LOS 5 -15 and -25 -15 show peaks at about 490 nm and 438 nm respectively which cannot be explained at this point and need further investigations.
- The polarization correction is unable to solve the 430 and 480-490 nm peaks in the EVs. LOS 5-15 shows more differences from the rest when polarization correction is turned off.
- The impact of using a high order polynomial is larger than the polarization correction. Using the low order polynomial in the fit increases the LOS dependency where LOS 5-15 stands out from the rest. It will be interesting to investigate how much this LOS contributes to the difference of east-west scans.

### **OCIO residuals:**

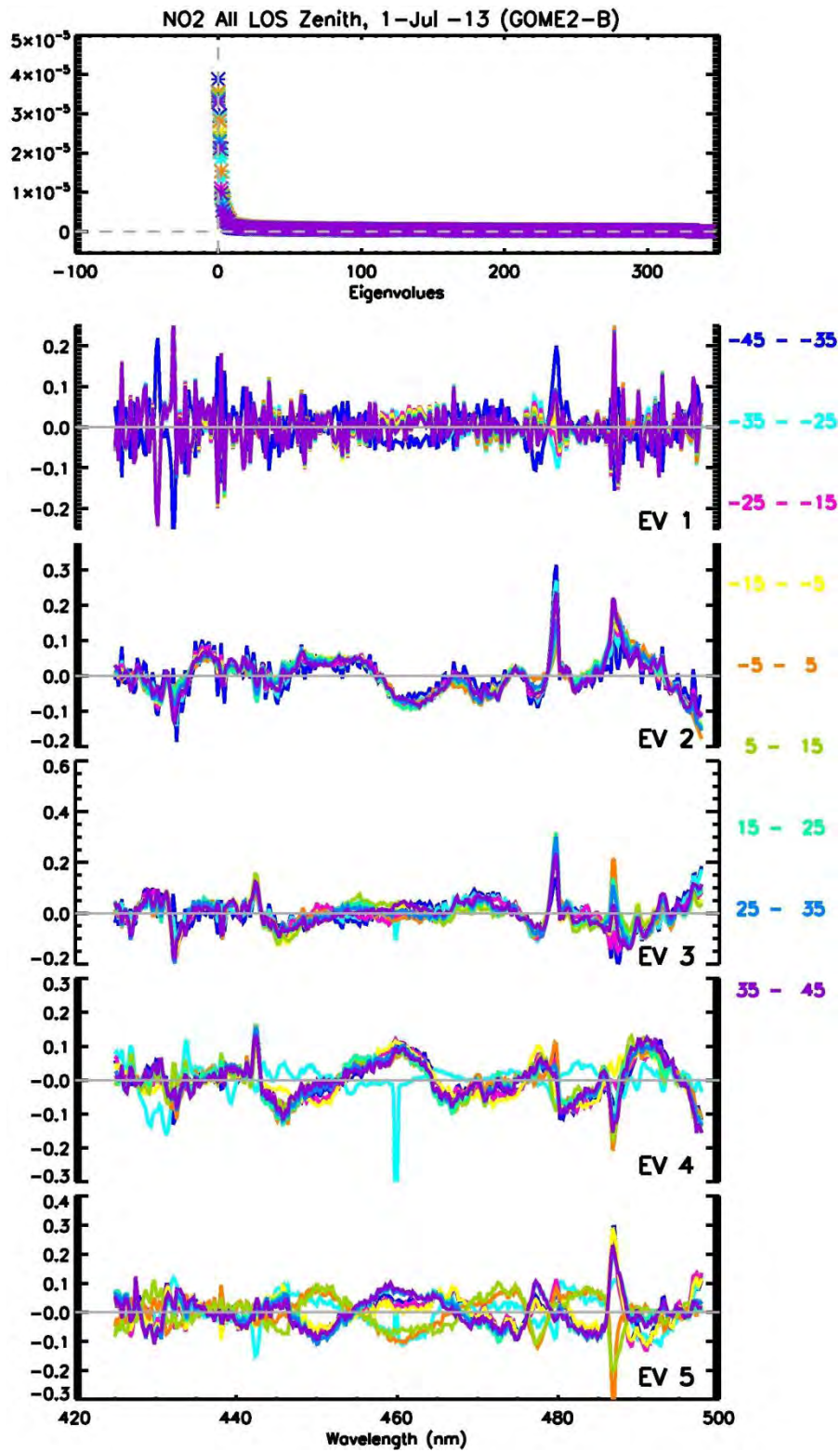
- For OCIO, PCA application and the interpretation of the results is more challenging due to the higher sensitivity of this species to the retrieval as well as calibration issues. Polarization correction is apparently more critical in this channel compared to the NO<sub>2</sub>.

PCA conducted on selected case studies lead to the identification of some calibration as well as fit problems. The observations confirmed the results obtained from the residuals study for the respective cases in other part of this project addressing the subject of detection of degradation and calibration issues. Regarding the second question, PCA can help to improve on the calibration procedure provided the analysis is performed in many steps where the results are used as predictors for selection criterion for the subsets in the subsequent analysis.

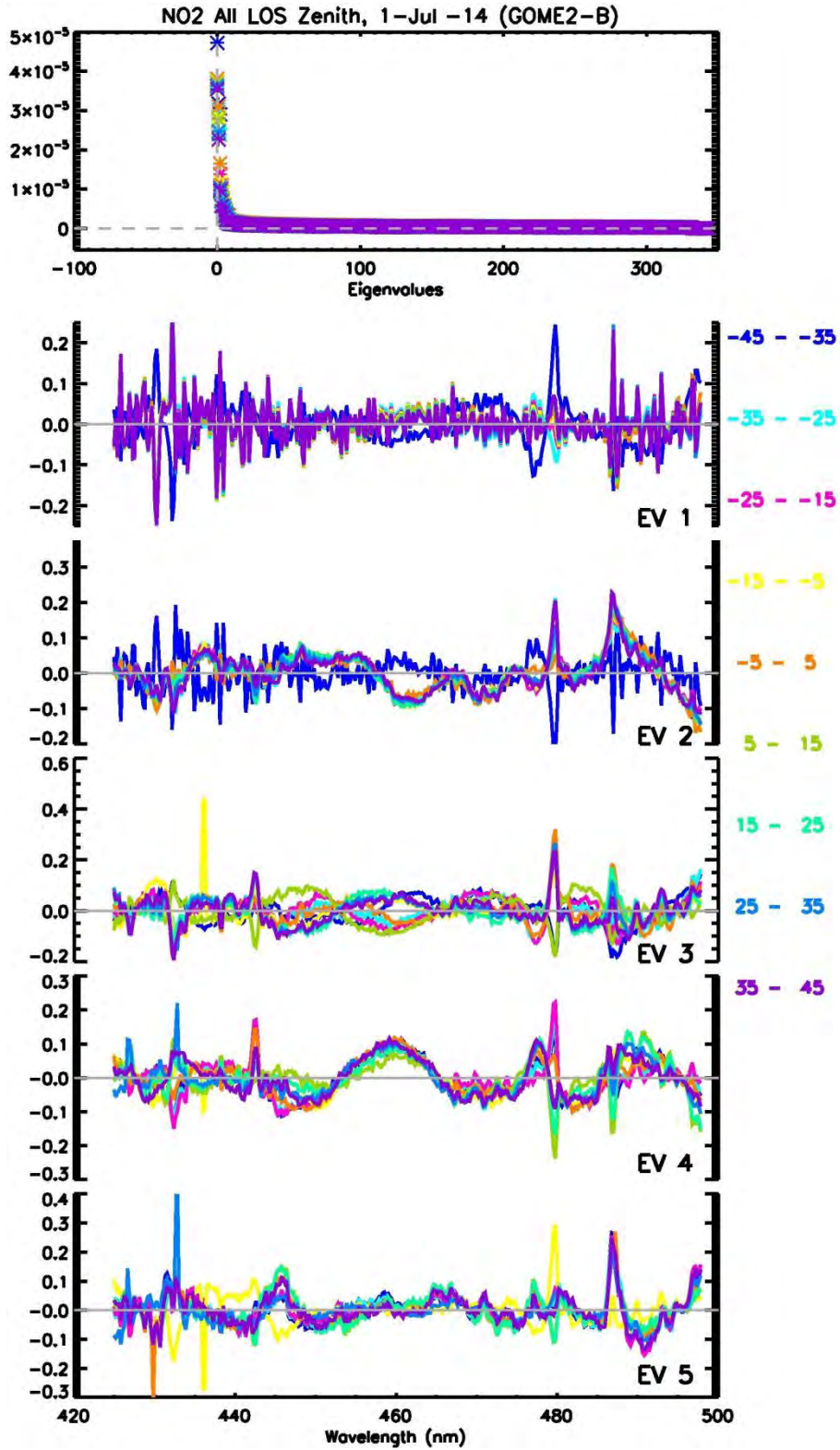
## 8 Appendix



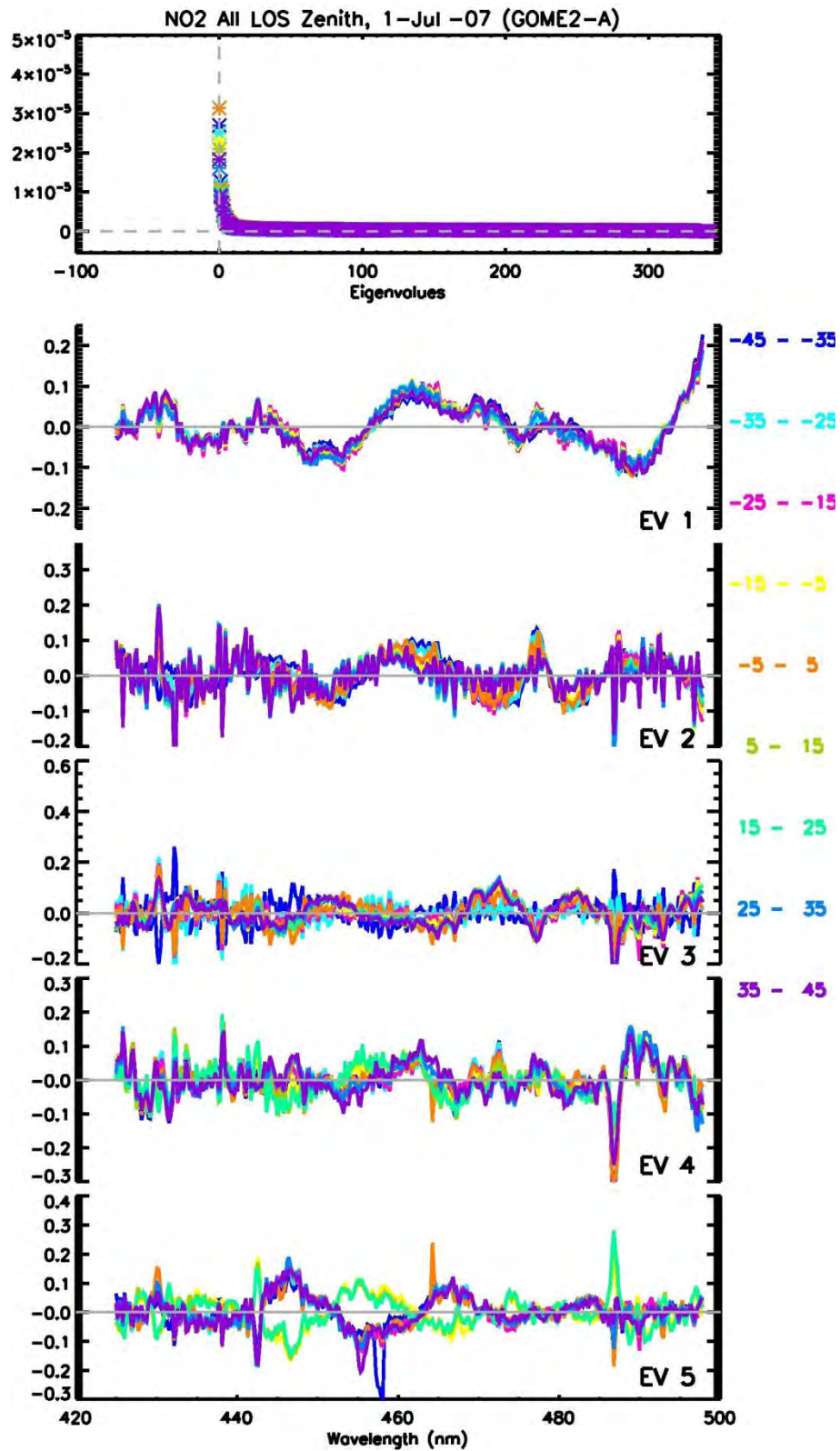
A1: PCA results for the GOME2-A and GOME2-B NO<sub>2</sub> residuals (425-495nm, x-axis) for the 1<sup>st</sup> Jan. and 1<sup>st</sup> Jul. values for the tropic subset.



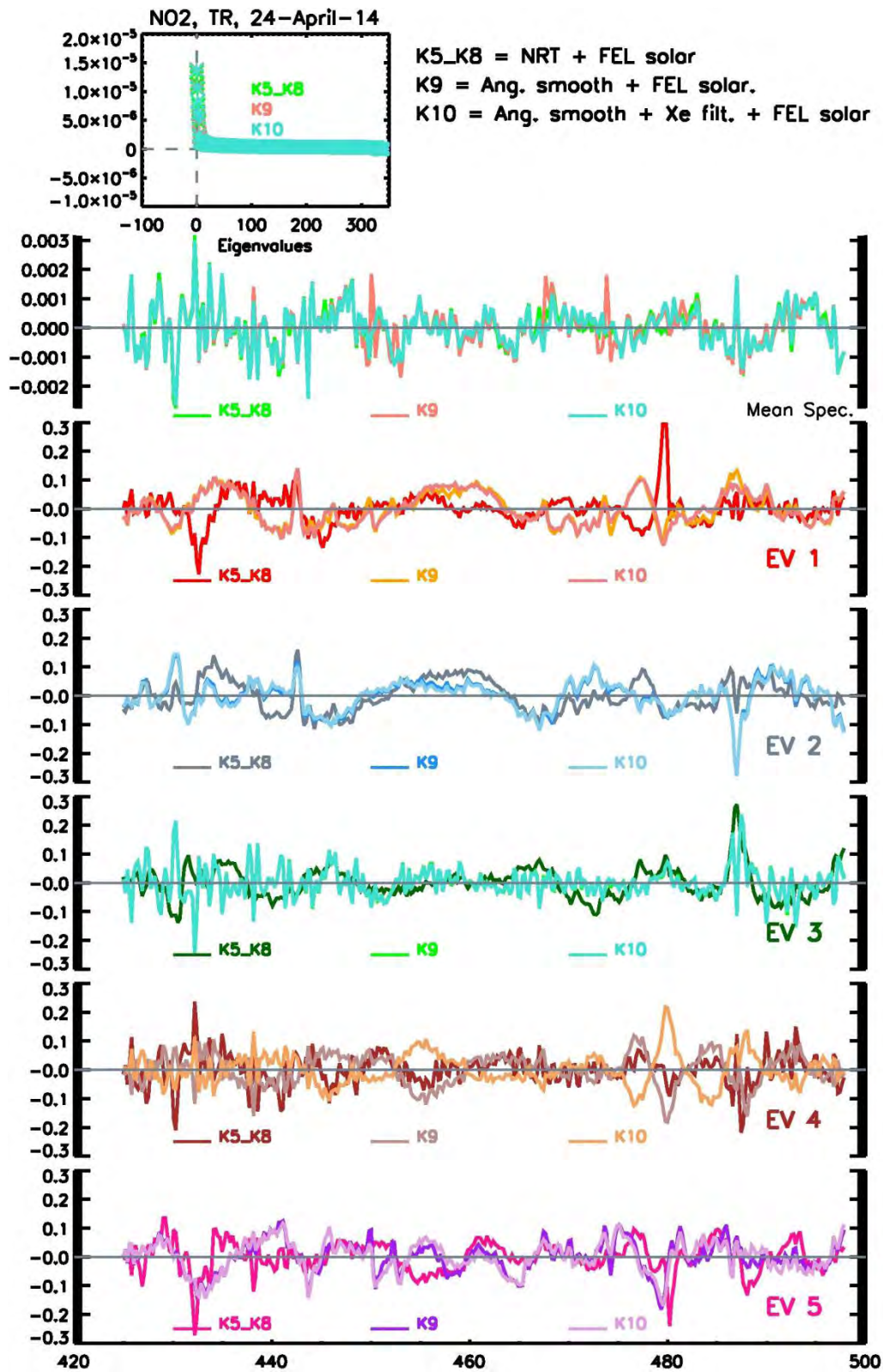
**A2a:** PCA results for NO<sub>2</sub> residuals (425-495nm, x-axis) for the GOME2-B, 1<sup>st</sup> Jul. 2013 values for 9 LOS subsets.



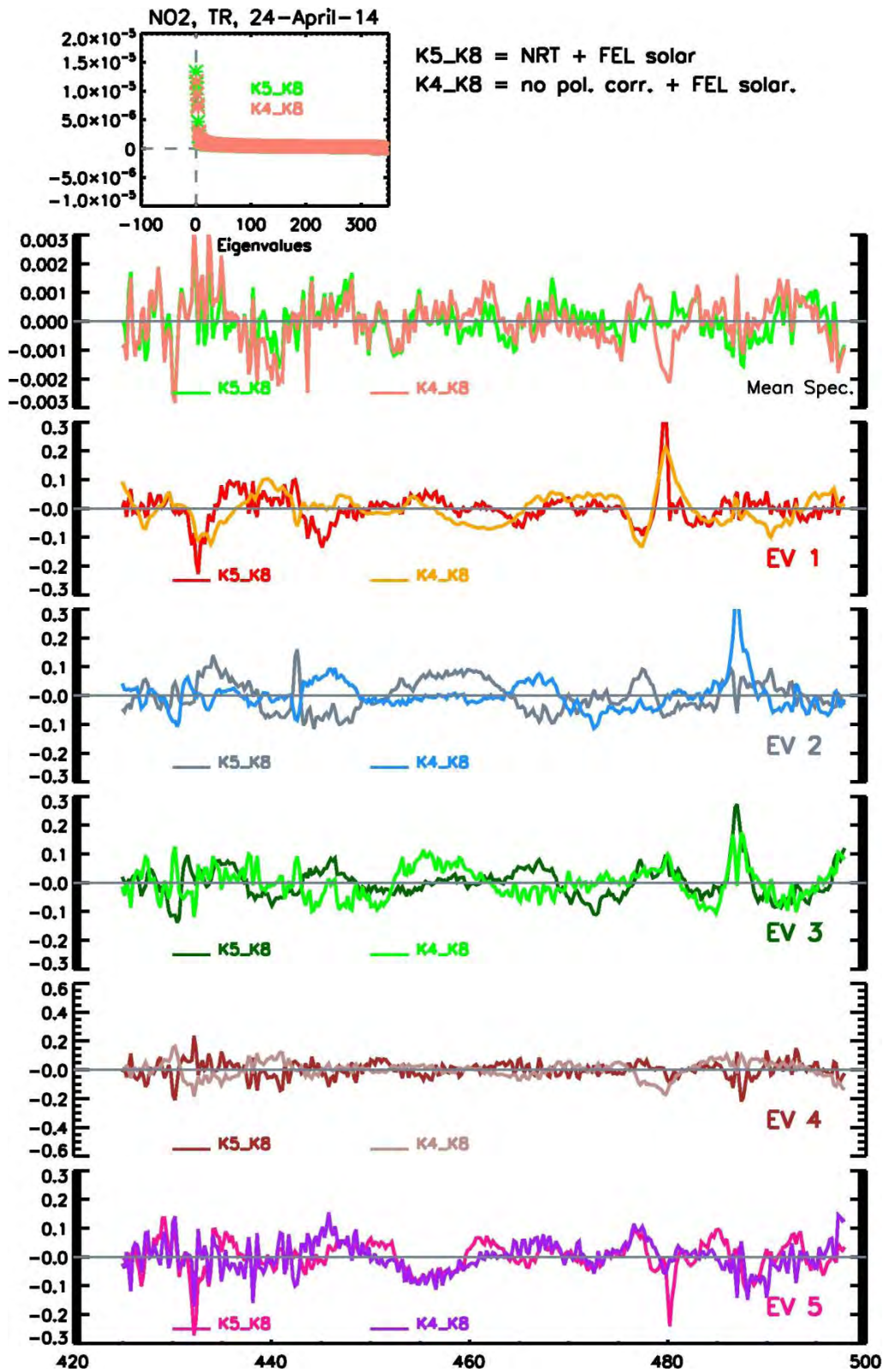
**A2b:** PCA results for NO<sub>2</sub> residuals (425-495nm, x-axis) for the GOME2-B, 1<sup>st</sup> Jul. 2914 values for 9 LOS subsets.



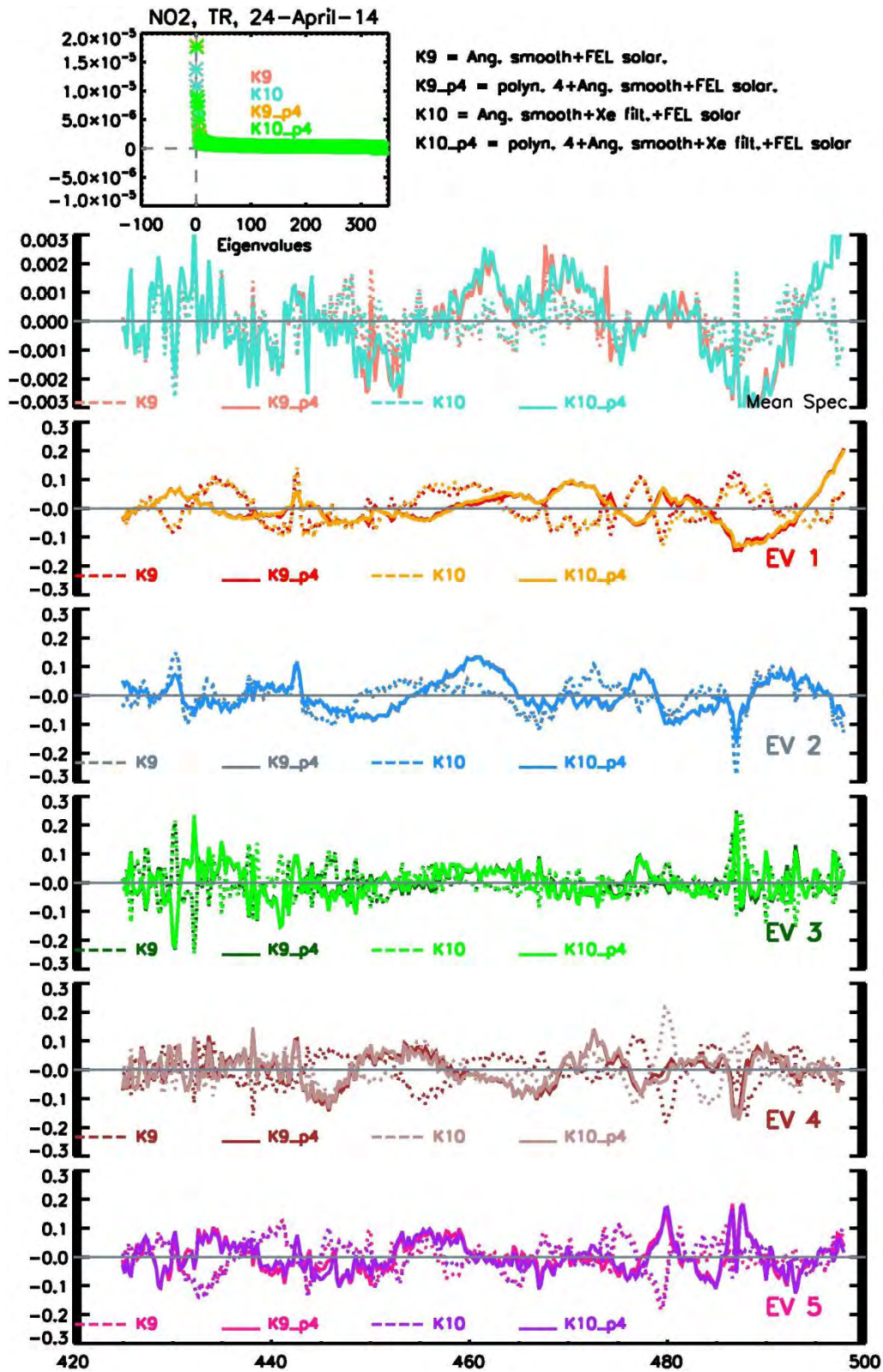
**A2c:** PCA results for NO<sub>2</sub> residuals (425-495nm, x-axis) for the GOME2-A, 1<sup>st</sup> Jul. 2007 values for 9 LOS subsets.



A3: PCA result for the improved keydata combinations K5\_K8, K9 and K10 for the tropics subset



A4: PCA result for the improved keydata combinations for the polarization impact for the tropical subset, K4\_K8 is with polarization being turned off, the results are compared to K5\_K8.



**A5:** PCa result for the improved keydata combinations for the low order polynomial impact for the tropics subset. K9\_p4 and K10\_p4 are with polynomial of degree 4, the results are compared to K9 and K10.